

Collider Search Constraints on Singlet-Doublet Fermionic Dark Matter Model

A Thesis

submitted to

Indian Institute of Science Education and Research Pune

in partial fulfillment of the requirements for the

BS-MS Dual Degree Programme

by

Saurabh Vasant Kadam



Indian Institute of Science Education and Research Pune

Dr. Homi Bhabha Road,
Pashan, Pune 411008, INDIA.

April, 2018

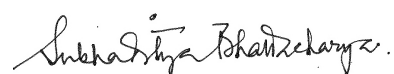
Supervisor: Dr. Subhadya Bhattacharya

© Saurabh Vasant Kadam 2018

All rights reserved

Certificate

This is to certify that this dissertation entitled Collider Search Constraints on Singlet-Doublet Fermionic Dark Matter Model towards the partial fulfilment of the BS-MS dual degree programme at the Indian Institute of Science Education and Research, Pune represents study/work carried out by Saurabh Vasant Kadam at Indian Institute of Science Education and Research under the supervision of Dr. Subhaditya Bhattacharya, Assistant Professor, Department of Physics, IIT Guwahati, during the academic year 2017-2018.



Dr. Subhaditya Bhattacharya

Committee:

Dr. Subhaditya Bhattacharya

Dr. Arun Thalapillil

This thesis is dedicated to all the taxpayers, whose money I have used for everything.

Declaration

I hereby declare that the matter embodied in the report entitled Collider Search Constraints on Singlet-Doublet Fermionic Dark Matter Model are the results of the work carried out by me at the Department of Physics, IIT Guwahati, Indian Institute of Science Education and Research, Pune, under the supervision of Dr. Subhadya Bhattacharya and the same has not been submitted elsewhere for any other degree.

Saurabh Vasant Kadam

Acknowledgments

The Master's thesis is supposed to be the foundational step towards independent research initiating the path towards the Ph.D. From my experience, I can confirm on this. I am extremely grateful towards my mentor, Dr. Subhaditya Bhattacharya, IIT Guwahati, for his support and guidance. He allowed me to freely explore the problem so that I could learn from experience and think independently. I am also thankful to his Ph.D. students, Basabendu Berman and Purushottam Ghoshal who helped me understand the technicalities of the project. I extend my gratitude towards IIT Guwahati for their hospitality. I am thankful to Dr. Arun Thalapillil, IISER Pune for his guidance. My family played an important role of supporting me. I thank Brijesh for accompanying me almost every day for an evening tea at the banks of Brahmaputra. I am also thankful to YouTube and Netflix for refreshing my mind. Finally, I extend my gratitude towards Mitali, Rajeev, Shruti, Swanand and Mrunal who kept me sane and never let me feel detached from IISER.

Abstract

Dark matter (DM) physics is one of the major areas of recent particle physics research. Even after finding hints from rotational curves, inhomogeneities in CMBR, bullet cluster and indirect evidence from astrophysics, the exact nature of DM is still unknown. Particle physics research for DM has been guided by postulating DM primarily as a weakly interacting massive particle (WIMP) which freezes out from equilibrium distribution in the early universe and contributes to the observed relic density. The spin of the DM is completely unconstrained.

In this thesis, we took up a minimal fermionic mixing DM model of a standard model(SM) $SU(2)$ singlet and a doublet that already has been proposed in the literature ¹ and updated the allowed parameter space under relic density criteria and recent direct search experiment, PandaX ². We studied in details the prospect of discovering it at the Large Hadron Collider for multilepton final state with 2, 3 and 4 leptons using monte carlo simulation methods. The analysis is done for few benchmark points in the parameter space allowed by relic density and direct detection criteria. We obtained that this model is very difficult to detect in future LHC runs at high luminosity due to heavy background from SM processes. But the significant region of the parameter space can still be tested for displaced charged vertex at LHC.

¹*K. Y. Lee, Y. G. Kim, and S. Shin*, Journal of High Energy Physics, vol. 2008, no. 05, p. 100, 2008

² Phys. Rev.Lett., vol. 119, p. 181302

Contents

Abstract	vi
1 Introduction	1
1.1 Dark Matter	1
1.2 WIMP Dark Matter	2
1.2.1 Direct Detection	3
1.2.2 Indirect Detection	4
1.2.3 Collider Search	5
2 Singlet-Doublet Fermionic Dark Matter Model	6
2.1 Standard Model	6
2.2 Singlet-Doublet Fermionic Dark Matter (SDFDM)	9
2.2.1 Model, Parameters and Interactions	10
3 DM Phenomenology of SDFDM	14
3.1 Relic Density and Direct Search	14
3.2 Results and Discussion for Relic Density Criteria and Direct Detection Search of SDFDM Model	19
4 Phenomenology at LHC	23

4.1	Collider Physics	23
4.1.1	Observables	25
4.1.2	Tools and Methodology	26
4.2	Collider search of SDFDM	27
4.3	Results and Discussion for Collider Searches of SDFDM Model	29
4.3.1	Event selection	33
5	Conclusions and Outlook	38
A	Weinberg-Salam Model	40
A.1	Electroweak Theory	40
A.2	Spontaneous Symmetry Breaking and Particle Masses	42
A.3	The Final Lagrangian	44
B	Additional Data	45
B.1	MicrOMEGA output of BP1	45
B.2	Distributions for all benchmark points	47
C	Scalar Triplet Extension to SDFDM model	50

List of Tables

2.1	Particles in standard model.	9
4.1	Benchmark points in SDFDM model chosen for collider search analysis	29
4.2	Dominant background from standard model processes	32
4.3	Effective number of events for multi-lepton final states. $L = 1000 \text{ fb}^{-1}$	34
4.4	Standard model background for multi-lepton final states. $L = 1000 \text{ fb}^{-1}$	34

List of Figures

1.1	Direct search	3
1.2	Indirect search	4
1.3	Collider search	5
3.1	Dominant annihilation processes	15
3.2	$\psi_1 \bar{\psi}_2$ co-annihilation processes	16
3.3	$\bar{\psi}_1 \psi^-$ co-annihilation processes	16
3.4	$\bar{\psi}^+ \psi^-$ co-annihilation processes	17
3.5	Feynman diagrams of $\psi_2 \psi^-$ decaying into dark matter ψ_1	17
3.6	Annihilation and co-annihilation processes to standard model fermions ($f\bar{f}$)	18
3.7	Dark matter nucleon interactions	19
3.8	Relic density vs. dark matter mass M_1 for different mass splittings $\Delta M = 50$ GeV, 200 GeV and mixing angles $\sin \theta = 0.1, 0.2, 0.3$	20
3.9	Solutions to Boltzmann equation for dark matter mass $M_1 = 400$ GeV, mass splitting $\Delta M = 500$ GeV and mixing angles $\sin \theta = 0.05, 0.10, 0.20$	21
3.10	Mixing angle $\sin \theta$ vs dark matter mass M_1 parameter space with relic density satisfying points and direct search constraint from PandaX-II	22
4.1	Definition of polar and azimuthal angle along beam pipe	24
4.2	Feynman diagrams showing leptonic final state events for SDFDM model in collider searches.	30

4.3	Lepton transverse momentum (p_T), missing transverse energy (MET) and dilepton invariant mass (m_{ll}) distributions of a SDFDM model benchmark point	32
4.4	Significance plots for benchmark points	35
4.5	Mixing angle $\sin\theta$ vs. dark matter mass M_1 parameter space for possible displaced vertex signal at LHC, along with relic density criteria and direct search constraints from PandaX-II	37
B.1	Missing transverse energy (MET) distributions for all benchmark points . . .	47
B.2	Lepton transverse momentum (p_T) distributions for all benchmark points . .	48
B.3	Dilepton invariant mass (m_{ll}) distributions for all benchmark points	49
C.1	Lepton transverse momentum (p_T), missing transverse energy (MET) and dilepton invariant mass distributions (m_{ll}) for a benchmark point in the scalar triplet extension to SDFDM model, allowed by relic density and direct detection constraints	51

Chapter 1

Introduction

1.1 Dark Matter

The era of dark matter (DM) began when it was first proposed by Fritz Zwicky in 1933, as some non-luminous matter to explain the velocity distribution of galaxies in the Coma cluster [1]. Since then, there is plenty evidence for the existence of dark matter, many of which are even from very recent times. The early history of dark matter physics is summarized here [2]. Some of the notable astrophysical observations before 1980 confirming the presence of non-luminous matter are [3], [4], [5] and the work by Ostriker and Peebles [6] where the authors solved the problem of instabilities in the galactic disks by proposing a spherical halo of dark matter around the galaxies. In recent times, the X-ray spectroscopy [7] and the gravitational lensing [8] methods turned out to be the clear observations of dark matter. These methods were used later in the observation of the Bullet cluster which was formed by the collision of two large galaxy clusters. It was seen that the luminous mass, which was detected by the X-ray spectroscopy, lags behind the total mass, which was calculated by gravitational lensing, and a huge chunk of non-luminous mass passes through the luminous mass without much hindrance [9]. Due to the excellent agreement with Bullet cluster observations [10], the Weakly Interacting Massive Particle (WIMP) dark matter models are so popular. Finally, the measurement of the acoustic peaks in the Cosmic Microwave Background (CMB) measured by COBE [11], WMAP [12] and PLANCK [13] satellites put a constraint on the relic density contribution from the dark matter. Further evidence comes from the requirement of dark

matter in cosmology to generate the density perturbations that led to large-scale structures [14] and to account for big bang nucleosynthesis [15]. [16] and [17] discuss viable dark matter candidates like sterile neutrino, axions, etc.

In this work, we have studied a WIMP model of vector-like singlet doublet fermionic dark matter. In chapter 2 we have reviewed the standard model (SM) content and built up the model in beyond SM scenario. In chapter 3 we have discussed the phenomenology of DM in the context of relic density criteria and direct detection experiments. chapter 4 contents our main work of collider constraints on this model along with basics of collider physics and its methodologies.

We briefly summarize the WIMP DM and its experimental status.

1.2 WIMP Dark Matter

The early Universe was a hot dense mixture of particles and the interaction rate for all the species prevailed over the expansion rate, causing everything to stay intact. As it cooled down, different species decoupled (froze out) from the plasma at different times depending upon the strength of their interaction with others. In the present time, decoupled stable species appears as a relic and its abundance depends upon the temperature at which it decoupled.

From the anisotropies in the cosmic microwave background radiation (CMBR), it is known that the DM is a relic, making up around 23% of the universe [13]. This relic abundance of DM, Ω_{DM} , depends upon the its thermally averaged annihilation cross section times velocity, $\langle\sigma_{ann}v\rangle$ as $\Omega_{DM} \sim \frac{2 \times 10^{-26} \text{ cm}^3/\text{s}}{\langle\sigma_{ann}v\rangle}$ [18].

Weakly Interacting Massive Particle (WIMP) dark matter models are based on the particles (ϕ) with masses around the weak scale mass $M_\phi \sim 100 \text{ GeV}$ and the interaction strength g_ϕ near weak scale interaction strength $g_\phi \sim g_{weak} \sim 0.6$. The $\langle\sigma_{ann}v\rangle$ for WIMP particles is roughly equal to $10^{-6} \frac{m_\phi^2}{g_\phi^4} \text{ GeV}^{-2}$. The relic abundance of such particles turns out to be near the observed dark matter relic density $\Omega_{DM} \sim 0.2$. It so happens that this mass lies within the mass range, 100 GeV to 1 TeV, where the current particle physics experiments are designed to look for new physics. This coincidence is known as the WIMP miracle, and

this made WIMP models so popular among theorists [19].

Apart from the strongly suggested existence of DM from astrophysical and cosmological observations, we have no other information about its characteristics like spin, mass, etc. There are various ongoing experiments which are designed to detect and determine the properties of DM but none of them has detected it. We summarize prominent experimental methodologies, 1. Direct detection. 2. Indirect detection. 3. Collider search. , and the experiments based on them in the following sections.

1.2.1 Direct Detection

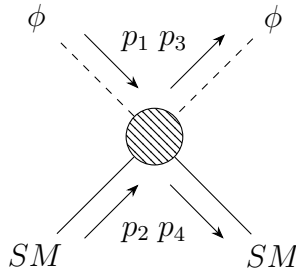


Figure 1.1: Direct detection

The cosmological observations mentioned in the beginning of this chapter have made the existence of dark matter evident. Due to its huge abundance, it is safe to assume that the earth is passing through a cosmic shower of DM. The direct detection experiments are set up to measure the interaction of these DM particles with some target nuclei (Figure 1.1). The detectors measure signals produced by elastic collision between DM particles and target nuclei. Usually the signals are heat produced due to phonon excitations, scintillation photons emitted from the de-excitation of nuclei after the collision or direct ionization of target nuclei. To distinguish between the scattering of interest and the background signals, the experiments are designed to collect the data from combination of two detection channels as the relative size of the signals depend upon the types of interacting particles.

A complete review on direct detection methods is given in [20]. Current (2017) status in direct dark matter detection experiments is summarized in [21]. Some of the established direct detection experiments are LUX [22], PandaX-II [23], XENON100 [24], XMASS [25], DEAP-3600 [26], SuperCDMS [27], CDEX [28], DAMIC [29], CRESST [30], PICO [31] etc.

1.2.2 Indirect Detection

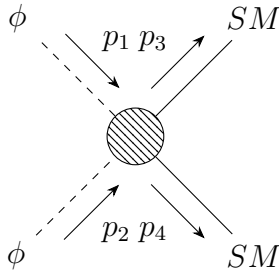


Figure 1.2: Indirect detection of DM annihilation

Indirect detection methods operate on astrophysical scales and hence can detect the effects of very weak processes, which are otherwise undetectable with ground base experiments. According to [32], there are three methods of indirect detection and two of them (γ ray probe and charged cosmic ray probe) are based on the consequences of DM annihilation to SM particles (Figure 1.2) while the remaining one (neutrino telescope) is just observing large scale effects of direct detection like processes (Figure 1.1). Being a relic, DM can't spontaneously annihilate into visible matter at current temperature, but the observational effects in indirect methods are usually from the galactic halo of DM trapped in the gravity of massive structures. In such halo, fraction of DM particles acquire enough energies to annihilate into SM particles. On the Universal scale this is a local phenomenon and thus does not affect the relic abundance, yet can be large enough to detect with current equipment.

In the γ ray probe method, spectral features of direct annihilation of DM into photons (from tree level or loop level processes) or the virtual internal bremsstrahlung are compared with the signals from the gamma ray sources like Galactic centre of pulsar. Experiments based on this method are, Fermi Large Area Telescope (Fermi-LAT) [33], HESS [34], MAGIC [35] and VERITAS [36]. Measurement of positron to electron ratio is very sensitive and could change to measurable extent due to DM annihilating into antiparticles. Such excess in positrons is measure in PAMELA [37] and AMS [38] experiments to determine the bounds on DM annihilation cross section. Neutrino spectroscopy measures the excess in solar neutrinos produced by DM hydrogen interaction. The abundant hydrogen inside the Sun makes solar neutrino searches very sensitive to spin-dependent part of the DM-nucleon cross section. The instruments for neutrino searches are IceCube [39] and ANTARES [40].

1.2.3 Collider Search

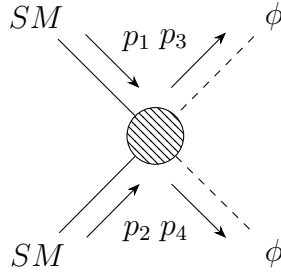


Figure 1.3: Collider search

Collider search experiment try to detect the possible production of DM by colliding the SM particles (Figure 1.3). These experiments can be lepton colliders or hadron colliders. We will specifically look into the hadron colliders as the energy of collision in such experiments is of order TeV which can produce particles of having mass of few hundreds of GeV. Also, in circular lepton collider a large amount of energy is lost due to accelerating charges in the form of bremsstrahlung radiations. In Large Hadron Collider (LHC) [41], two beams of proton with relativistic velocities are collided after accelerating them in a circle of radius 27 km where the centre of mass energy is $\sqrt{s} = 13$ TeV [42]. This makes LHC the largest particle accelerator.

WIMP searches are done by usual methods of searching new physics at LHC which starts by constructing a Lagrangian and new particle content. The cross section of production of such particles is then calculated using their interactions from Lagrangian which determines the probability of production. A final state signal is determined to look for, generated by this new physics. Signals are determined by the particles in the final state, which can be either leptons or hadrons (section 2.1). These signals are then checked for any excess on top of known SM background. To reduce the SM background event selection criteria are imposed on final state signal by using the observables constructed from particle momentum and energy, which are measurable. Parameter space of DM model is then contained by excess found for such signals at LHC.

Chapter 2

Singlet-Doublet Fermionic Dark Matter Model

In an attempt to explain the nature of DM constrained to the observations mentioned in §1.1, particle physicist extend the well established theory of fundamental particles, the SM, by adding one or many particles subjected to existing or new symmetries. Such scenario is called beyond standard model physics (BSM). In this chapter, we will first summarize the standard model and its symmetries. Later, we will introduced the dark sector as BSM particles.

2.1 Standard Model

The fundamental constituents of matter known to us by probing the energies of order TeV are leptons and quarks, which are fermions with spin $1/2$. There are three generations of quarks and leptons. Each generation of leptons come in pairs with one charged lepton (electron (e^-), muon (μ^-), tau (τ^-)) and its neutral partner (electron neutrino (ν_e), muon neutrino (ν_μ), tau neutrino (ν_τ)). Similarly, each generation of quarks come in pairs: up and down (u, d), charm and strange (c, s) and top and bottom (t, b) with up versions of each pair has charge $+2/3$ and down version of each pair has charge $-1/3$.

Among four forces in the nature, strong force, weak force, electromagnetic force and

gravitational force, the SM incorporates first three forces and ignores the last one for particle interactions. Each of these three forces is mediated by spin 1 vector bosons described by some gauge theories. Strong force is mediated by 8 gluons (g), weak force is mediated by 3 vector bosons (W^\pm, Z^0) and electromagnetic force is mediated by the photon (γ). Quarks interact through all three forces, while leptons interact through weak and electromagnetic forces. Such protected interactions and multiplets of particles are explained by imposing transformation laws on particles under certain symmetries. The SM is described by $SU_C(3) \otimes SU_L(2) \otimes U_Y(1)$ symmetry. Here $SU(N)$ is a group of special unitary transformations on N objects, the subscripts C, L and Y stand for Color, Left and (weak) hypercharge, which we will explain later. The $SU(3)$ part describes strong interaction where its 8 generators are 8 gluons. The $SU_L(2) \otimes U_Y(1)$ part describes the electroweak (unified electromagnetic and weak) interactions where the $3 + 1$ generators are linear combinations of W^\pm, Z^0 and γ .

Leptons are excluded from the strong interactions by making them color singlet, i.e. invariant under $SU_C(3)$, while quarks are color triplet and thus can have interaction terms with gluons such that the Lagrangian still remains invariant. Each quark comes in three colors (r, g, b), which is a “three-dimensional” analog of charge for strong force. The gluons are massless which makes strong force a long range force, yet we never observe strong force in low energy scales like gravity or electromagnetic force. This is because the strength of strong force increases with distance and thus the only stable configurations of quarks are color singlets, either 3 quark bound states known as baryons (e.g. proton (uud), neutron (udd)) or 2 quark bound states known as mesons (e.g. pion ($u\bar{d}$)).

Unlike the strong force, the multiplet nature of electroweak theory has a very interesting empirical feature of parity violation. The left and right handed components of particles, which are given by

$$\psi_L = \frac{1 - \gamma^5}{2} \psi, \quad \psi_R = \frac{1 + \gamma^5}{2} \psi \quad (2.1)$$

with $\psi = \psi_L + \psi_R$, where ψ is a fermion field, interact differently under electroweak force. The right handed component plays no role in electroweak interaction. This is depicted by restricting the $SU(2)$ symmetry of electroweak force for left components of lepton and quarks. This explains the L subscript in $SU_L(2) \otimes U_Y(1)$. The left handed components of quarks and leptons form a doublet under $SU_L(2)$, e.g. $\begin{pmatrix} \nu_e \\ e \end{pmatrix}_L$, and thus can have interactions with the $SU(2)$ gauge bosons, W^\pm and Z^0 , while keeping the Lagrangian invariant. The doublet is indexed by weak isospin (t_3) with upper components - $u_L, c_L, t_L, (\nu_e)_L, (\nu_\mu)_L, (\nu_\tau)_L$ having

$t_3 = 1/2$ and lower components - $d_L, s_L, b_L, e_L^-, \mu_L^-, \tau_L^-$ having $t_3 = -1/2$. The right handed singlet fields have $t_3 = 0$. The charge associated with $U_Y(1)$ is called (weak) hypercharge and it is assigned differently to left and right handed components. The electric charge is related to weak isospin and hypercharge as

$$Q = t_3 + \frac{Y}{2} \quad (2.2)$$

The gauge bosons of $SU_L(2)$, W^+, W^0 and W^- , are triplet with isospin $t_3 = +1, 0, -1$ respectively, while the gauge boson of $U_Y(1)$, B^0 , being a generator of an abelian group does not carry hypercharge or weak isospin.

The theory given above, although describes all the interactions observed, doesn't allow to write mass terms of vector boson in the Lagrangian to protect the gauge symmetries, which makes weak force long range contradictory to experimental observation. Also the parity violation forbids us to write a fermion mass term as left and right handed components in mass term $\bar{\psi}\psi$ transform differently. This implies that the real world is not explained by rich underlying symmetry but by some lower form of it. This is achieved by the mechanism of Spontaneous Symmetry Breaking (SSB) which breaks the higher symmetry group of $SU_L(2) \otimes U_Y(1)$ into lower $U_{em}(1)$ symmetry group, while keeping the $SU_C(3)$ untouched. It is done by adding a $SU_L(2)$ doublet complex scalar field (H), known as Higgs Field. The potential of this new field is adjusted by tuning the interaction parameters such that the stable ground state of this field is non-trivial. Because of this, H gets a non-zero expectation value with the ground state. Thus, all three particle interaction terms with such Higgs field reduce to two particle terms in the Lagrangian, when the Higgs field is expanded about the non-zero vacuum expectation value, which are precisely the mass terms. The particle content of SM is summarized in [Table 2.1](#) [43].

Details of Higgs mechanism and particle masses along with mathematical formalism of electroweak theory is given in [Appendix A](#).

Particle	Q	t_3	Y	Color
u_L, c_L, t_L	2/3	1/2	1/3	triplet
d_L, s_L, b_L	-1/3	-1/2	1/3	triplet
$(\nu_e)_L, (\nu_\mu)_L, (\nu_\tau)_L$	0	1/2	-1	singlet
e_L^-, μ_L^-, τ_L^-	-1	-1/2	-1	singlet
u_R, c_R, t_R	2/3	0	4/3	triplet
d_R, s_R, b_R	-1/3	0	-2/3	triplet
e_R^-, μ_R^-, τ_R^-	-1	0	-2	singlet
8 gluons	0	0	0	octet
W^\pm	± 1	± 1	0	singlet
W^0	0	0	0	singlet
B^0	0	0	0	singlet
H	1, 0	$\pm 1/2$	1	singlet

Table 2.1: Particles in standard model.

2.2 Singlet-Doublet Fermionic Dark Matter (SDFDM)

In beyond standard model (BSM) situation, adding $SU(2)$ n -multiplets to the standard model whose lightest neutral component, which is thus stable, can be a dark matter candidate. Multiplets with $Y \neq 0$ are excluded as DM candidates, even their stability is assured by the presence of extra symmetry, because the large Z -mediated DM-nucleon elastic cross section makes them suffer a heavy parameter space loss by direct search constraints. Multiplets with hypercharge (Y) zero are stable by themselves for $n \geq 5$, while singlet and triplet need extra symmetry for their stability [44]. The singlet lepton (χ^0) with zero hypercharge, whose stability is assured by being odd under Z_2 symmetry, is a minimal possibility for a candidate of DM. We need to introduce additional fields (scalar singlet or vector like lepton doublets) to write renormalizable interaction terms with SM.

In this chapter we study the latter possibility of additional vector-like lepton doublet $\psi^T \equiv (\psi^0, \psi^-)$ along with a fermionic singlet χ^0 which was proposed in [45]. The DM is admixture of neutral component of doublet ψ^0 and the singlet χ^0 .

2.2.1 Model, Parameters and Interactions

We introduce a $SU(2)$ fermion doublet $\psi^T \equiv (\psi^0, \psi^-)$ and a fermion singlet χ^0 , both singlet under $SU(3)$. ψ has hypercharge ($Y = -1$) and χ^0 has zero hypercharge ($Y = 0$). This causes the doublet to have a neutral component ψ^0 and a charged component $\psi^-(\bar{\psi}^+)$. Additionally, both ψ and χ^0 are odd under a discrete Z_2 symmetry, while all other fields are even under this new symmetry. Unlike SM, there is no evidence of parity violation in dark sector and hence the doublet introduced here transforms under $SU(2)$ for both left and right handed component and thus called vector-like. This immediately means that we can explicitly write a Dirac mass term for ψ .

To make the Lagrangian invariant, all terms must be even under Z_2 . Thus, new terms in the Lagrangian are the mass terms for both of these fields and the Z_2 invariant Yukawa couplings with the SM fields. Similar to the quark mass terms shown in the Appendix A.18, $[Y_k \bar{\psi} \tilde{H} \chi^0 + h.c.]$ are the only possible renormalizable Yukawa interactions with such constraints. Here, $\tilde{H} = i\tau_2 H^*$ and $H = (H^+, H^0)^T$ is SM Higgs field and Y_k is Yukawa coupling.

Thus the DM Lagrangian is

$$\mathcal{L}_{DM} = i\bar{\psi}\gamma^\mu D_\mu\psi - M_\psi\bar{\psi}\psi + i\bar{\chi}^0\gamma^\mu\partial_\mu\chi^0 - M_\chi\bar{\chi}^0\chi^0 - [Y_k\bar{\psi}\tilde{H}\chi^0 + h.c.] \quad (2.3)$$

where covariant derivative D_μ is given in Appendix A.8. After the electroweak phase transition, Higgs field H is expanded about its vacuum expectation value $\langle H \rangle = (0, v/\sqrt{2})^T$ as

$$H = \frac{1}{\sqrt{2}} \begin{pmatrix} 0 \\ v + h \end{pmatrix}$$

With this we get,

$$\mathcal{L}_{DM} = i\bar{\psi}\gamma^\mu D_\mu\psi - M_\psi\bar{\psi}\psi + i\bar{\chi}^0\gamma^\mu\partial_\mu\chi^0 - M_\chi\bar{\chi}^0\chi^0 - \frac{1}{\sqrt{2}}[Y_k v \bar{\psi}^0 \chi^0 + Y_k \bar{\psi}^0 h \chi^0 + h.c.] \quad (2.4)$$

This suggests a mixing between ψ^0 and χ^0 . The mass matrix in the basis (χ^0, ψ^0) is given by

$$\begin{pmatrix} M_\chi & m_D \\ m_D & M_\psi \end{pmatrix} \quad (2.5)$$

where $m_D = Y_k v / \sqrt{2}$. The characteristic equation for this matrix is

$$x^2 - (M_\psi + m_\chi)x + (M_\psi M_\chi - m_D^2) = 0$$

with eigenvalues

$$M_1 = \frac{M_\psi + M_\chi}{2} - \frac{M_\psi - M_\chi}{2} \sqrt{1 + \frac{4m_D^2}{(M_\psi - M_\chi)^2}} \quad (2.6)$$

$$M_2 = \frac{M_\psi + M_\chi}{2} + \frac{M_\psi - M_\chi}{2} \sqrt{1 + \frac{4m_D^2}{(M_\psi - M_\chi)^2}} \quad (2.7)$$

$$(2.8)$$

We will assume $m_D \ll M_\psi, m_\chi \implies \sqrt{1 + \frac{4m_D^2}{(M_\psi - M_\chi)^2}} \approx 1 + \frac{2m_D^2}{(M_\psi - M_\chi)^2}$, which we will justify in §3. The mass eigenvalues are then,

$$M_1 \approx M_\chi - \frac{m_D^2}{M_\psi - M_\chi} \quad (2.9)$$

$$M_2 \approx M_\psi + \frac{m_D^2}{M_\psi - M_\chi} \quad (2.10)$$

with mass eigenstates

$$\psi_1 = \cos \theta \chi^0 + \sin \theta \psi^0 \quad (2.11)$$

$$\psi_2 = \cos \theta \psi^0 - \sin \theta \chi^0 \quad (2.12)$$

where the mixing angle θ is defined by

$$\tan 2\theta = \frac{2m_D}{M_\psi - m_\chi} \quad (2.13)$$

The charged vector-like fermion have mass

$$M_\psi \simeq M_1 \sin^2 \theta + M_2 \cos^2 \theta = M^\pm \quad (2.14)$$

Since $m_D \ll M_\psi, M_\chi$, θ is very small. This means ψ_1 is dominantly a singlet and ψ_2 is dominantly a doublet. Also in this limit $\tan 2\theta \approx \sin 2\theta = \frac{2Y_k \nu}{\Delta M}$ where $\Delta M = M_\psi - M_\chi \simeq M_2 - M_1$. This indicates that the model has three independent parameters. We choose them

to be $\Delta M, M_1$ and $\sin \theta$. For $\Delta M > 0$, the mass M_1 is the smallest mass and ψ_1 is the lightest particle, which makes it a DM candidate.

We can find the interaction vertex factors by rewriting the Lagrangian in terms of ψ_1 and ψ_2 by solving (2.11) and (2.12) and using Appendix A.14 and Appendix A.13.

$$\begin{aligned} \mathcal{L}_{DM}^{int} = & \frac{g}{2 \cos \theta_W} [\cos^2 \theta \bar{\psi}_2 \gamma^\mu Z_\mu \psi_2 + \sin^2 \theta \bar{\psi}_1 \gamma^\mu Z_\mu \psi_1 - \sin \theta \cos \theta (\bar{\psi}_1 \gamma^\mu Z_\mu \psi_2 + \bar{\psi}_2 \gamma^\mu Z_\mu \psi_1)] \\ & - \frac{g}{\sqrt{2}} \sin \theta \bar{\psi}_1 \gamma^\mu W_\mu^+ \psi^- + \frac{g}{\sqrt{2}} \cos \theta \bar{\psi}_2 \gamma^\mu W_\mu^+ \psi^- + \frac{g}{\sqrt{2}} \sin \theta \bar{\psi}^+ \gamma^\mu W_\mu^- \psi_1 \\ & - \frac{g}{\sqrt{2}} \cos \theta \bar{\psi}^+ \gamma^\mu W_\mu^- \psi_2 + g \sin \theta_W \bar{\psi}^+ \gamma^\mu A_\mu \psi^- + \frac{g}{2 \cos \theta_W} \cos 2\theta_W \bar{\psi}^+ \gamma^\mu Z_\mu \psi^- \\ & + \frac{Y_k}{\sqrt{2}} h [\sin 2\theta (\bar{\psi}_1 \psi_1 + \bar{\psi}_2 \psi_2) - \cos 2\theta (\bar{\psi}_1 \psi_2 + \bar{\psi}_2 \psi_1)] \end{aligned}$$

This gives interactions with Higgs,

$$\begin{aligned} \begin{array}{c} \bar{\psi}_1 \\ \nearrow \\ \psi_1 \end{array} \cdots h &= \frac{Y_k}{\sqrt{2}} \sin 2\theta & \begin{array}{c} \bar{\psi}_2 \\ \nearrow \\ \psi_2 \end{array} \cdots h &= -\frac{Y_k}{\sqrt{2}} \sin 2\theta & \begin{array}{c} \bar{\psi}_{1,2} \\ \nearrow \\ \psi_{2,1} \end{array} \cdots h &= \frac{Y_k}{\sqrt{2}} \cos 2\theta \end{aligned} \quad (2.15)$$

and interactions with vector bosons,

$$\begin{aligned} \begin{array}{c} \bar{\psi}_1 \\ \nearrow \\ \psi_1 \end{array} \cdots Z_\mu &= \frac{g \sin^2 \theta}{2 \cos \theta_W} \gamma^\mu & \begin{array}{c} \bar{\psi}_2 \\ \nearrow \\ \psi_2 \end{array} \cdots Z_\mu &= \frac{g \cos^2 \theta}{2 \cos \theta_W} \gamma^\mu & \begin{array}{c} \bar{\psi}_{1,2} \\ \nearrow \\ \psi_{2,1} \end{array} \cdots Z_\mu &= \frac{g \sin \theta \cos \theta}{2 \cos \theta_W} \gamma^\mu \end{aligned} \quad (2.16)$$

$$\begin{aligned} \begin{array}{c} \bar{\psi}_1(\bar{\psi}_2) \\ \nearrow \\ \psi^- \end{array} \cdots W_\mu^+ &= \frac{g \sin \theta (\cos \theta)}{\sqrt{2}} \gamma^\mu & \begin{array}{c} \bar{\psi}^+ \\ \nearrow \\ \psi_1(\psi_2) \end{array} \cdots W_\mu^+ &= \frac{g \sin \theta (\cos \theta)}{\sqrt{2}} \gamma^\mu \end{aligned} \quad (2.17)$$

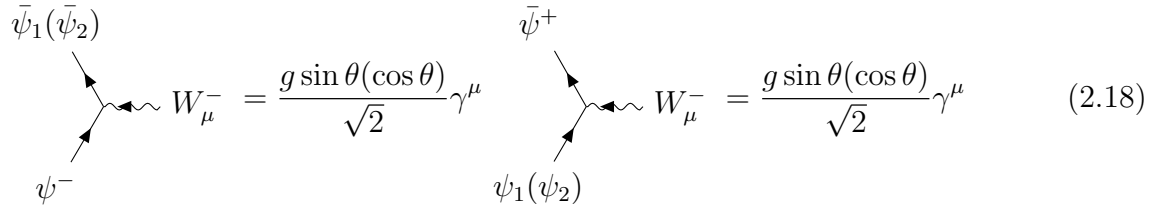


Diagram (2.18) shows two Feynman diagrams for the coupling of a W^- boson to fermions. The left diagram shows an incoming fermion ψ^- and an outgoing antifermion $\bar{\psi}_1(\bar{\psi}_2)$ meeting at a vertex connected to a W^- boson. The right diagram shows an incoming fermion $\psi_1(\psi_2)$ and an outgoing antifermion $\bar{\psi}^+$ meeting at a vertex connected to a W^- boson. Both diagrams are associated with the coupling $\frac{g \sin \theta (\cos \theta)}{\sqrt{2}} \gamma^\mu$.

$$\bar{\psi}_1(\bar{\psi}_2) \quad \psi^- \quad W^-_\mu = \frac{g \sin \theta (\cos \theta)}{\sqrt{2}} \gamma^\mu \quad \bar{\psi}^+ \quad \psi_1(\psi_2) \quad W^-_\mu = \frac{g \sin \theta (\cos \theta)}{\sqrt{2}} \gamma^\mu \quad (2.18)$$

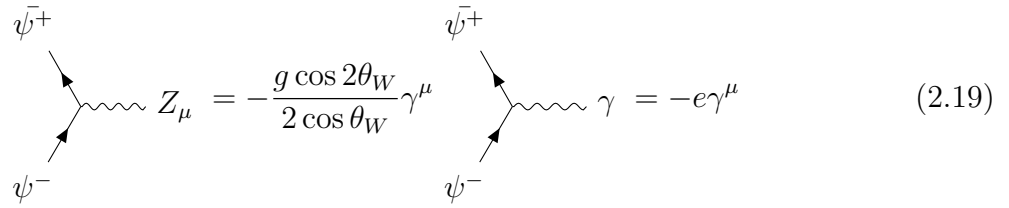


Diagram (2.19) shows two Feynman diagrams for the coupling of a Z boson and a photon to fermions. The left diagram shows an incoming fermion ψ^- and an outgoing antifermion $\bar{\psi}^+$ meeting at a vertex connected to a Z boson. The right diagram shows an incoming fermion ψ^- and an outgoing antifermion $\bar{\psi}^+$ meeting at a vertex connected to a photon γ . The Z boson coupling is $-\frac{g \cos 2\theta_W}{2 \cos \theta_W} \gamma^\mu$ and the photon coupling is $-e \gamma^\mu$.

$$\bar{\psi}^+ \quad \psi^- \quad Z_\mu = -\frac{g \cos 2\theta_W}{2 \cos \theta_W} \gamma^\mu \quad \bar{\psi}^+ \quad \psi^- \quad \gamma = -e \gamma^\mu \quad (2.19)$$

In the next chapter, we will put constraints on the parameter space from relic density criteria and direct search results.

Chapter 3

DM Phenomenology of SDFDM

3.1 Relic Density and Direct Search

The relic abundance of a certain species with density ρ is quantified by its relic density, Ωh^2 , which is given by

$$\Omega \equiv \frac{\rho}{\rho_C} \quad \rho_C \equiv \frac{3H^2}{8\pi G} \quad (3.1)$$

where H is the Hubble parameter, G is the Newton's constant and h is the uncertainty in Hubble parameter [46, ch. 1]. The current bounds on Ωh^2 for non-baryonic matter come from the measurements of anisotropies in Cosmic Microwave Background Radiation (CMBR) done by PLANCK satellite which are [13].

$$0.1133 \leq \Omega_{DM} h^2 \leq 0.1189 \quad (3.2)$$

The contribution to the relic abundance comes from the thermal averaged scattering amplitude times thermal velocity $\langle \sigma_A |v| \rangle$, which measures the strength of interaction of relic particle with all other species present in the plasma. For SDFDM model, the relic density

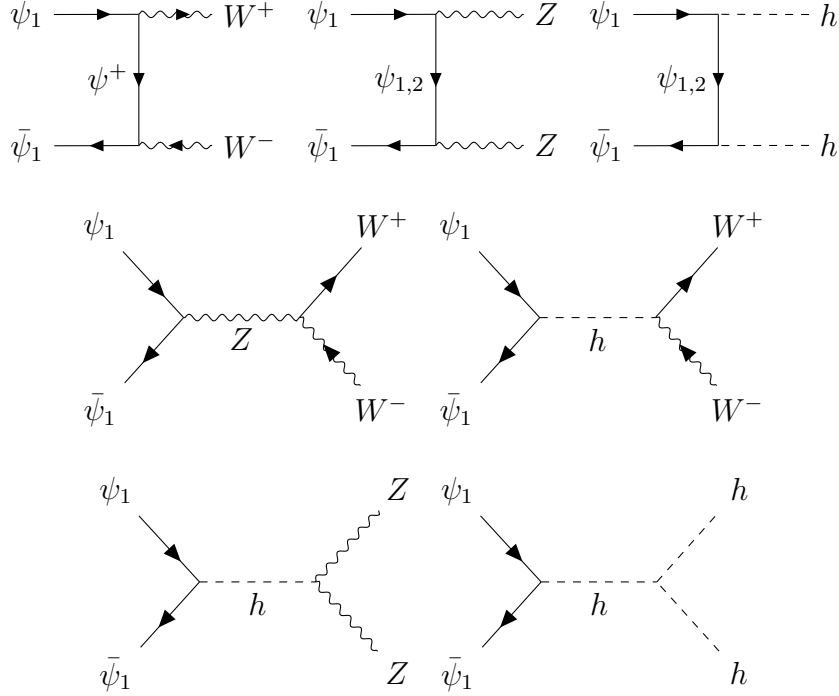


Figure 3.1: Dominant annihilation processes to Higgs and gauge boson final states

of ψ_1 DM of mass M_1 is given by [47]

$$\Omega_{\psi_1} h^2 = \frac{1.09 \times 10^9 \text{ GeV}^{-1}}{g_*^{1/2} M_{PL}} \frac{1}{J(x_f)} \quad (3.3)$$

where g_* is total number of effectively relativistic degrees of freedom, $M_{PL} = 1.22 \times 10^{19}$ and $J(x_f)$ is given by

$$J(x_f) = \int_{x_f}^{\infty} \frac{\langle \sigma |v| \rangle_{eff}}{x^2} dx$$

where $x = M_1/T$ and subscript f is for freeze out temperature. From this, it is clear that large scattering cross section will reduce the relic density and it agrees with our earlier discussion in [section 1.2](#) as large cross section means freeze out will occur at lower temperatures. In SDFDM model, the dominant contribution to the scattering amplitude comes from various types of reactions. One type of contribution is from the direct annihilation of DM candidate ψ_1 into SM particles, as shown in [Figure 3.1](#).

Second type of contribution is from the co-annihilation with other BSM particles, both charged (ψ^\pm) and massive chargeless (ψ_2) particles, into SM particles, as shown in [Figure 3.2](#)

and Figure 3.3 . Both of these processes are directly number changing processes. But such contributions depend upon the availability of interacting particles.

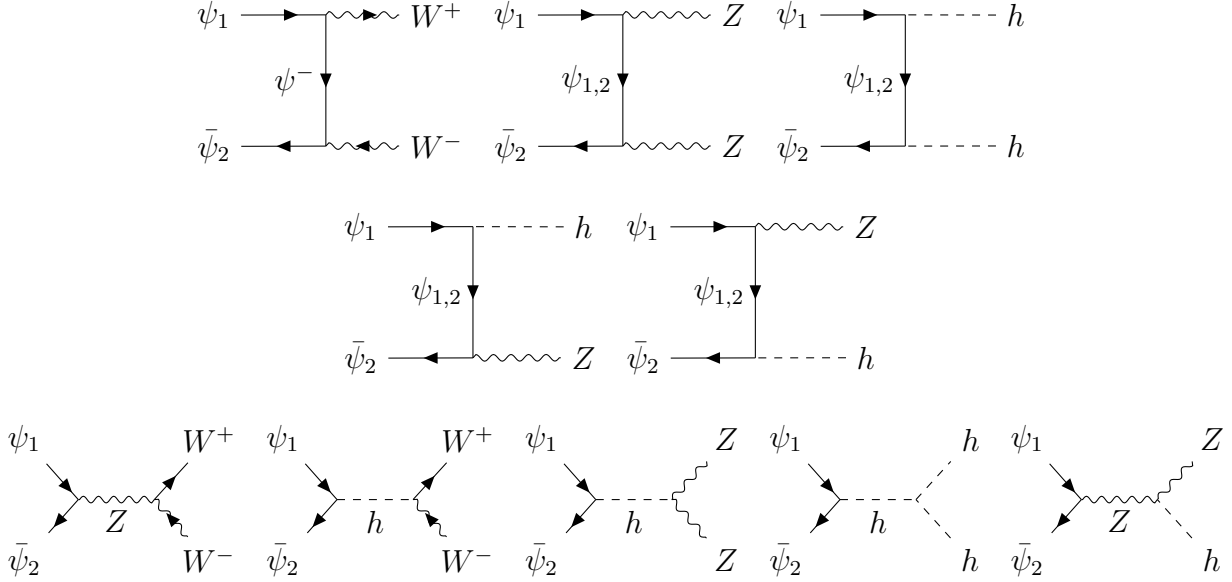


Figure 3.2: Dominant $\psi_1\bar{\psi}_2$ co-annihilation processes to Higgs and gauge boson final states

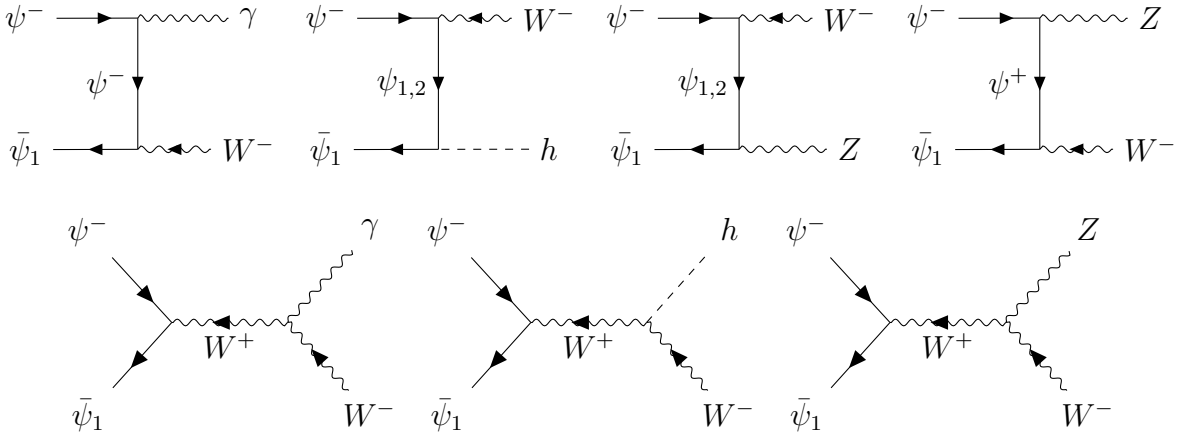


Figure 3.3: Dominant $\bar{\psi}_1\psi^-$ co-annihilation processes to Higgs and gauge boson final states

The third type of contribution plays an indirect role in freezing mechanism since it involves reactions in which non DM BSM particles (ψ_2, ψ^\pm) annihilate into SM particles (Figure 3.4, ψ_2 diagrams are similar to Figure 3.1) and this changes their availability for $\psi_1\psi^\pm$ or $\psi_1\psi_2$ co-annihilation as well as for the decay into ψ_1 (Figure 3.5).

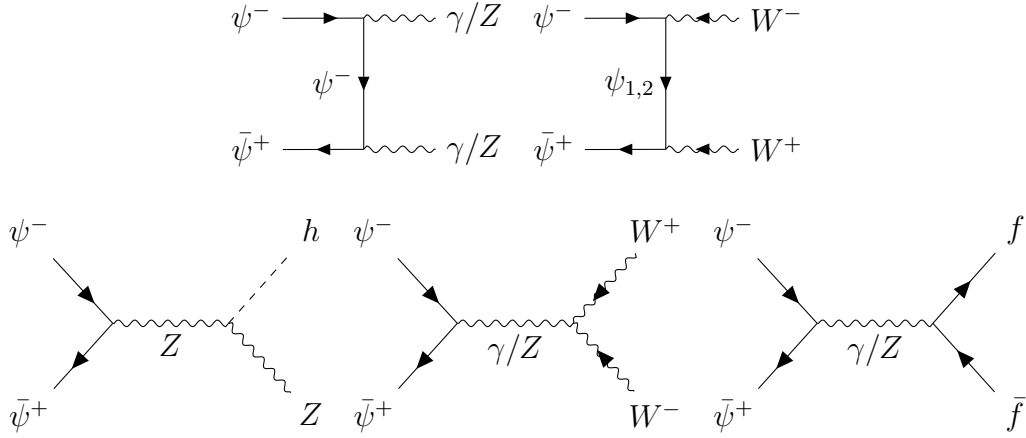


Figure 3.4: Dominant $\bar{\psi}^+\psi^-$ co-annihilation processes to Higgs and gauge boson final states

Here, we will justify the assumption we made in [subsection 2.2.1](#) of $\sin\theta \ll 1$. The mixing angle determines the doublet content in DM ψ_1 . With increasing doublet content, the annihilation cross section increases significantly through Z mediated $\psi_1\bar{\psi}_1 \rightarrow W^+W^-$ process because the interaction vertex with Z boson is proportional to $\sin^2\theta$ ([Equation 2.16](#)). This will increase the scattering cross section causing very small relic density. Later we will see that this increased cross section is strictly discarded by direct search experiments.

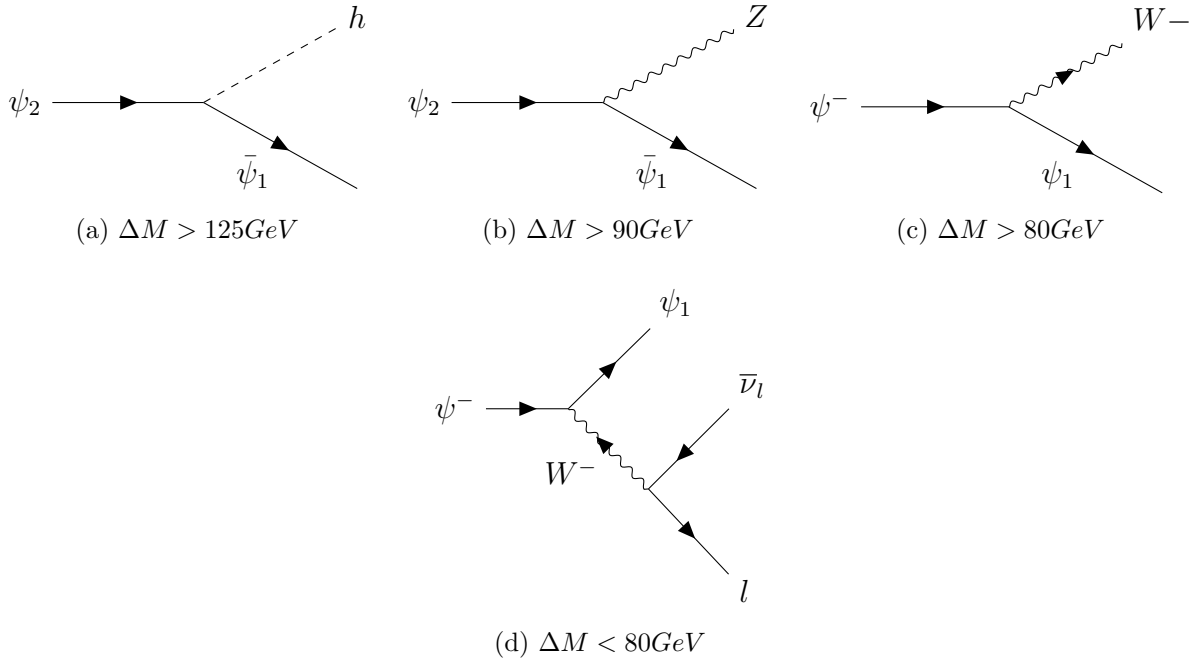


Figure 3.5: Feynman diagrams of $\psi_2 \psi^-$ decaying into DM ψ_1

In very small $\sin \theta$ regime where the direct annihilation is heavily suppressed, the decays of ψ_2, ψ^\pm play an important role in the relic abundance. The large presence of these particles will ensure co-annihilation with DM which will lower the relic abundance. Depending upon the mass splitting ΔM , decays of ψ_2, ψ^\pm shown in Figure 3.5 are possible. Increasing ΔM will increase the decay channels and thus the availability of these particles will reduce resulting in increased DM relic density.

Finally, very small contribution to the relic density calculation also comes from annihilation into SM fermions $f\bar{f}$.

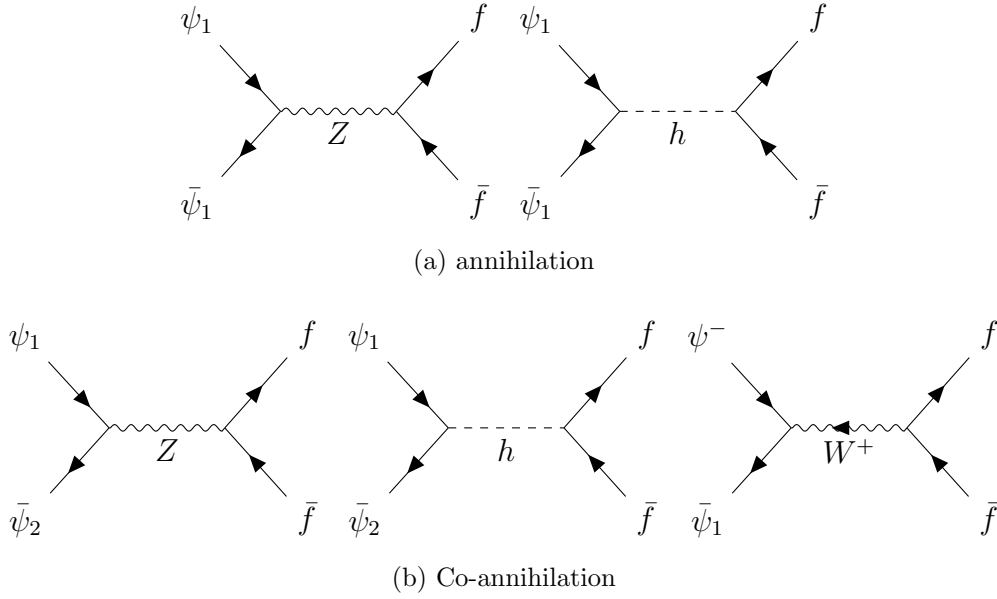


Figure 3.6: Annihilation and co-annihilation processes to SM fermion ($f\bar{f}$) final states. The contribution to scattering cross section from these processes is very less.

As explained in [subsection 1.2.1](#), the direct detection method depends upon the scattering cross section of DM with nucleons which are composed of SM fermions. The DM ψ_1 interacts with fermions through Z-boson and Higgs. Thus Figure 3.7 are the only possible Feynman diagrams.

The spin independent scattering cross section per nucleon varies with $\sin \theta$ as, [\[48\]](#)

$$\sigma_{SI}^Z \simeq 3.75 \times 10^{-39} \text{cm}^2 \sin^4 \theta \quad (3.4)$$

As mentioned earlier, the $\sin^4 \theta$ dependence in DM-nucleon cross section does not allow the large $\sin \theta$ possibility because it will increase this cross section significantly making the model

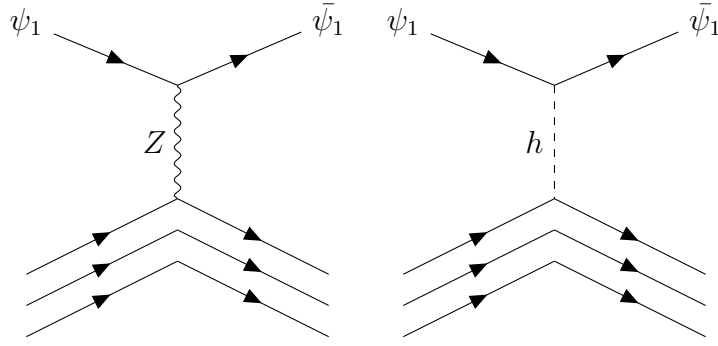


Figure 3.7: DM nucleon interactions. The three fermion line represent a nucleon.

detectable in the direct search experiments.

To study the allowed parameter space for this model, we have implemented the model in `MicrOMEGAS` [49] and scanned parameter space for points satisfying the relic density criteria and direct detection constraints in low $\sin \theta$ region.

3.2 Results and Discussion for Relic Density Criteria and Direct Detection Search of SDFDM Model

We have plotted the relic abundance for various $\sin \theta$ and ΔM values in Figure 3.8. With increasing $\sin \theta$, the relic density is seen to be decreasing which agrees with our discussion in section 3.1.

In both graphs, Figure 3.8a and Figure 3.8b, we can see the sudden drops around 45 GeV and 63 GeV, which correspond to Z boson resonance and Higgs resonance. Resonance in relic density plots is a common feature. For any direct annihilation diagrams, like Figure 3.1, if the annihilation process is s-channel with mediator X , then the cross section has a contribution of form $\frac{1}{(s-M_X)^2}$ from the propagator of mediating particle. The formalism of relic density calculation assumes s-wave annihilation i.e. the annihilating particles are almost stationary which implies $s = (p_1 + p_2)^2 = 4M_\psi^2$. When the particle mass M_ψ is close to half of the mass of mediator, the denominator tends to zero, increasing the scattering cross drastically and resulting in very low relic density. In our case the mediators are Z boson and Higgs boson, thus we see two resonance drops at $M_1 \simeq M_Z/2 = 45$ GeV and at $M_1 \simeq M_H/2 = 63$.

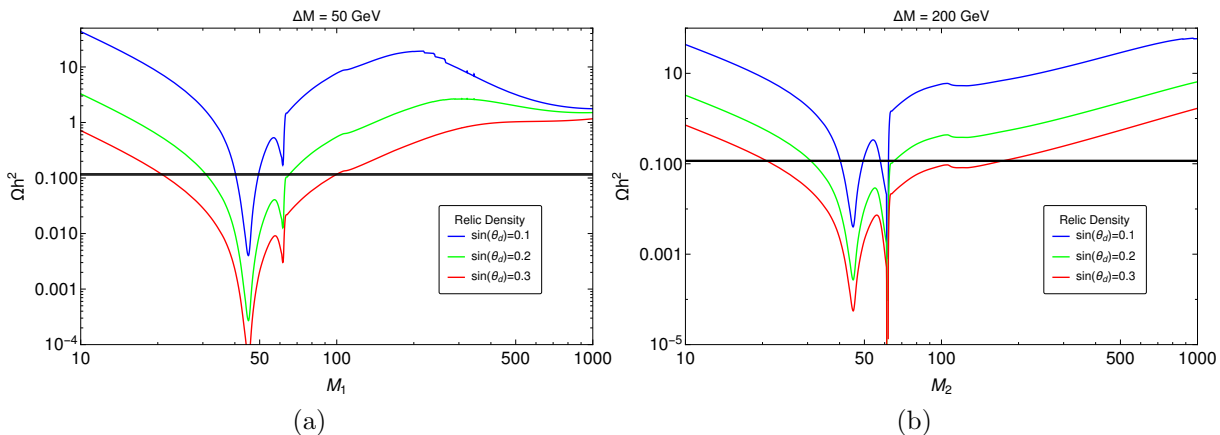


Figure 3.8: Relic density vs. dark matter mass M_1 for different $\Delta M = 50$ GeV, 200 GeV (left, right) and $\sin\theta = 0.1, 0.2, 0.3$ (Blue, Green, Red) values. The black band represents the bounds on relic density, $0.1133 \leq \Omega_{DM} h^2 \leq 0.1189$, given by PLANCK [13] data

For small ΔM splitting, the relic density decreases for $M_1 > 300$ GeV. This is because of the increasing $\bar{\psi}_2 \psi_1 \rightarrow SM$ $\psi^\pm \psi_1 \rightarrow SM$ co-annihilation contribution in the scattering cross section. On the other hand, this feature is not seen in Figure 3.8b. The co-annihilation region depends upon the rate of collisions with other DM BSM particles. Being in a thermal bath, this collision process is proportional to the Boltzmann factor and the Boltzmann factor decreases exponentially with increasing mass difference.

Thermal evolution of a species is given by the Boltzmann equation [46, pp. 126]

$$\frac{dY}{dx} = -\frac{x \langle \sigma_{\psi_1 \bar{\psi}_1 \leftrightarrow X \bar{X}} |v| \rangle s}{H(M_1)} [Y^2 - (Y_{EQ})^2] \quad (3.5)$$

$$H(M_1) \equiv \frac{1.67 \sqrt{g_*} M_1^2}{m_{Pl}} \quad (3.6)$$

$$Y \equiv \frac{n_{\psi_1}}{s} = \frac{n_{\bar{\psi}_1}}{s} \quad (3.7)$$

$$Y_{EQ} \equiv \frac{n_{\psi_1}^{EQ}}{s} = \frac{n_{\bar{\psi}_1}^{EQ}}{s} \quad (3.8)$$

where n_{ψ_1} is the number density of DM particle and s is the entropy of the universe at a given temperature. The subscript EQ is for equilibrium solution at that temperature. For a cold species, i.e. the species which freezes out at a temperature where its velocity is

non-relativistic, the Y_{EQ} as a function of $x = M_1/T$ is given by [46, 3.75]

$$Y_{EQ}(x) = \frac{45}{2\pi^4} \frac{g}{g_*s} \left(\frac{\pi}{8}\right)^{1/2} x^{3/2} e^{-x} \quad (3.9)$$

In Figure 3.9, we have plotted the thermal evolution of SDFDM particle by explicitly solving Equation 3.5 under s-wave approximation of $\langle\sigma_{\psi_1\bar{\psi}_1\leftrightarrow X\bar{X}}|v|\rangle$. To avoid the complication due to co-annihilation, we have kept ΔM large (500 GeV). The relic density $\Omega_{\psi_1}h^2$ calculated from Y_∞ as given in [46, 5.47, 5.48], which comes out as (50.24, 3.97, 0.30) respectively for (Blue, Green, Red). The values match closely with the MicrOMEGA results (42.98, 3.25, 0.25). We have plotted, using MicrOmega [49], the direct search cross section for varying DM mass

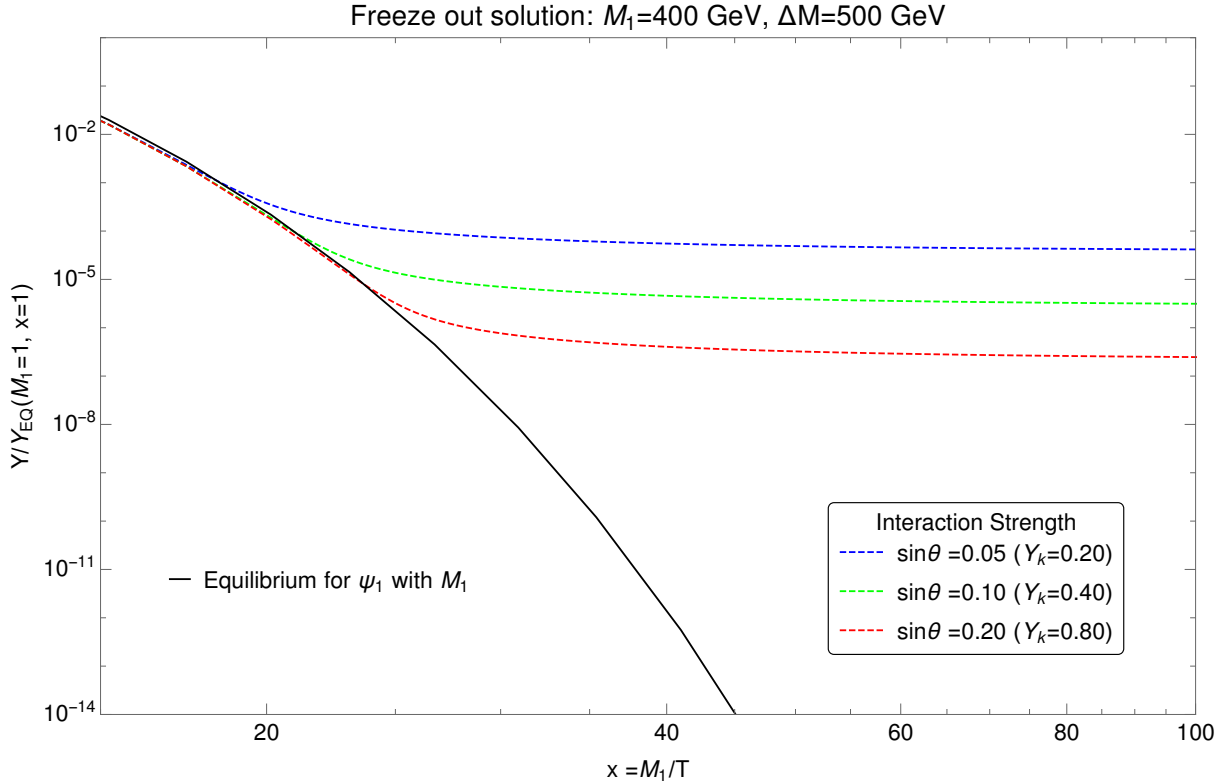


Figure 3.9: Solutions to Boltzmann equation are plotted for $M_1 = 400$ GeV and $\Delta M = 500$ GeV, for different interaction strengths $Y_k = (0.2, 0.4, 0.8)$, shown in (Blue, Green, Red) respectively. The Black line shows the Y_{EQ} , Y-axis is rescaled Y and X-axis is inversely proportional to temperature.

M_1 for different mixing angle values in Figure 3.10. The solid line indicates the PandaX-II [23] constraint. The discrete points satisfy relic density bounds mentioned in Equation 3.2.

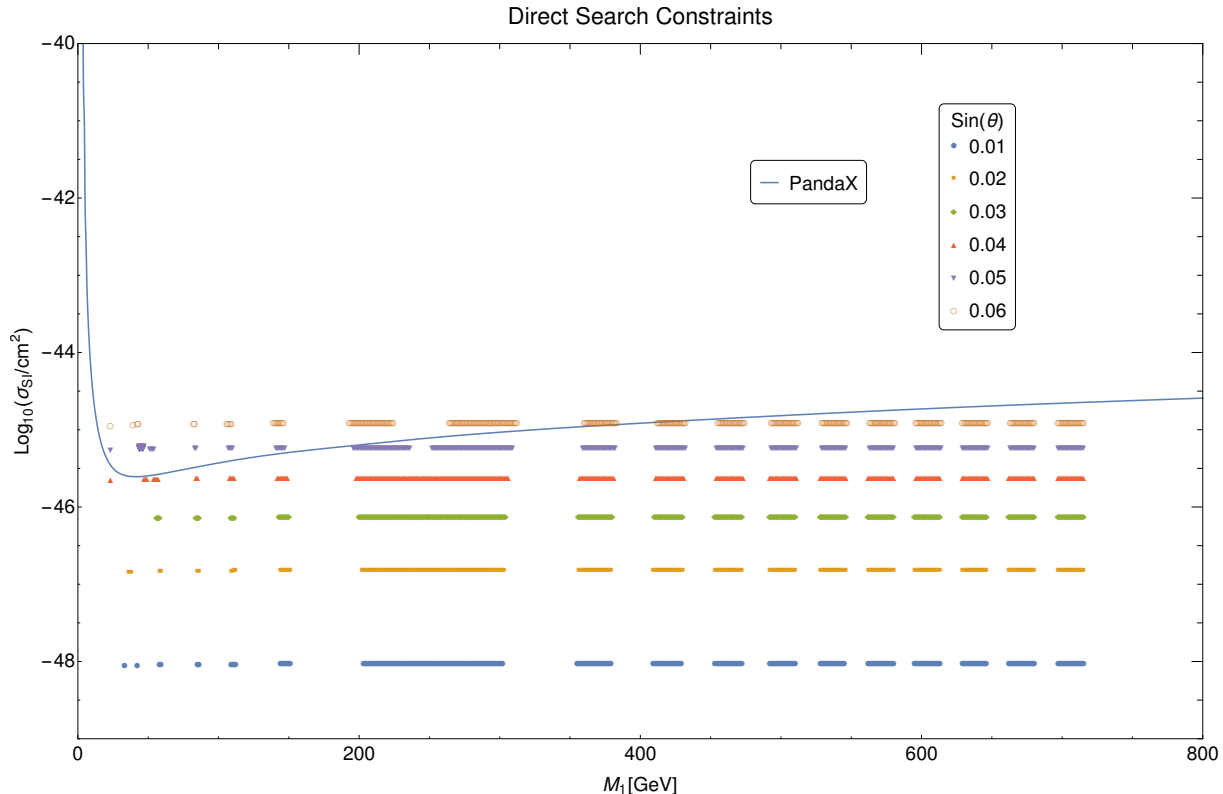


Figure 3.10: The blue line indicates PandaX-II [23] constraint. Discrete points are relic density satisfying points for various $\sin \theta$ values and ΔM varying from 1 GeV to 75 GeV (not shown). We can see DM-nucleon cross section increasing with $\sin \theta$

From Figure 3.10, we can clearly see that parameter space is heavily restricted by direct search constraint as $\sin \theta$ can't be greater than 0.06. On the other hand Figure 3.8 suggests that the relic density criteria requires larger $\sin \theta$.

One might think that the parameter space is thus exhausted significantly by direct search and relic density constraints. But here the co-annihilation comes to the rescue. For $\Delta M \approx 10$ GeV, the co-annihilation dominates at higher DM mass (as seen in Figure 3.8a) and reduces relic density drastically even for small $\sin \theta$ values which are allowed by direct search constraint.

Chapter 4

Phenomenology at LHC

SDFDM model has been extensively studied for available parameter space after relic density and direct detection constraints [48] [50]. We have discussed the analysis on the same in the last chapter. However, to our best knowledge, apart from few qualitative analysis [51], thorough and extensive analysis for collider search signatures of this model has not been done. In this chapter we will first summarize the general strategy for searching new physics at the LHC. Then, we will use it on the SDFDM model for few benchmark points in the parameter space allowed by relic density and direct detection.

4.1 Collider Physics

In LHC, the proton beam has large number of protons colliding head-on, giving rise to various final states. The number of collisions which give rise to a particular final states (an event) is proportional to the scattering cross section (σ) of that process. In collider physics, scattering cross section is measured in barn.

$$1\text{barn} = 1b = 10^{-24} \text{ cm}^2 = 2586 \text{ GeV}^{-2} \quad (4.1)$$

Another important quantity is instantaneous luminosity which is defined as number of collisions recorded per unit time per unit area. Integrated luminosity is time integration of instantaneous luminosity L which has a unit of 1/Area. The product of integrated luminos-

ity and production cross section of an event gives the effective number of events recorded over time. 2017 run of LHC had integrated luminosity of 50 fb^{-1} and is projected to reach at 2500 fb^{-1} in coming 10 years [52].

The relativistic proton beams are collided at different crossing points where detectors are placed which are designed according to the nature of experiment. The two very important experiments, ATLAS and CMS, are designed for searching new physics. Detectors there are constructed in layers where each layer detects and stores four momentum of certain type of particles [53]. The detector is cylindrical about the collision axis (beam pipe). Without going into the instrumentation and methods of detection, we will discuss the observables constructed from the measured variables, which will be used for event selection.

The detector measures four momentum of particle as $p^\mu = (E, p_x, p_y, p_z)$. By convention, z-axis is chosen along the beam pipe. The polar angle θ is defined with beam ends at $\theta = 0$ and $\theta = \pi$, $\theta = \pi/2$ being the direction perpendicular to the beam. Azimuthal angle $\phi \equiv \tan^{-1} p_x/p_y$ is measured along the cylindrical symmetry of beam pipe and varies from 0 to 2π Figure 4.1.

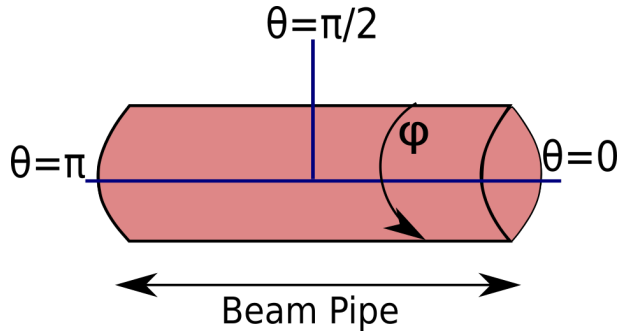


Figure 4.1: Polar angle θ and azimuthal angle ϕ

Instead of θ , the direction in polar plane is given by pseudorapidity which is given by

$$\eta \equiv \ln \cot \frac{\theta}{2} \quad (4.2)$$

$\eta = 0$ corresponds to direction perpendicular to beam pipe. Detectors can detect leptons with $\eta < 2.5$ which denotes the central region of detector in polar plane. Angular separation between two particles i and j is defined as

$$R_{ij} = \sqrt{(\phi_i - \phi_j)^2 + (\eta_i - \eta_j)^2} \quad (4.3)$$

For separately detecting two particles, minimum angular separation is required depending upon the nature of the particles.

4.1.1 Observables

Observables are constructed from particle four momentum and energy. They are used for checking the predictions of new physics by separating its signal from SM background. In our analysis we have used three observables for signal event selection criteria.

1. Missing Transverse Energy (MET, \cancel{E}_T)

The pp collision occurs in z direction. The particles have negligible momentum in x - y plane (transverse momentum, $\vec{p}_\perp = 0$) before collision, thus the final value of p_\perp is also zero as momentum is conserved in the plane perpendicular to the beam pipe. If some stable particles are produced during collision, which are not detectable by detectors, then they will carry away some momentum in x - y plane known as missing transverse momentum. Thus the vector addition of transverse momenta of all detected (visible) particles will be non-zero.

$$\vec{p}_\perp^{vis} + \vec{p}_\perp^{inv} = 0 \implies \vec{p}_\perp^{vis} = -\vec{p}_\perp^{inv}$$

The absolute value of this missing transverse momentum is known as missing transverse energy.

$$\cancel{E}_T = \left| \vec{p}_\perp^{vis} \right| \quad (4.4)$$

In SM, neutrinos are the only particles which leave the detector undetected and hence contribute to MET.

2. Transverse Momentum (p_T)

Transverse momentum of a particle is given by

$$p_T = |p_\perp| = \sqrt{p_x^2 + p_y^2} \quad (4.5)$$

3. Dilepton Invariant Mass (m_{ll})

Invariant mass or rest mass of a particle is a Lorentz invariant quantity given by $\sqrt{p^2} = \sqrt{p^\mu p_\mu} = \sqrt{E^2 - \vec{p}^2} = m$, where p^μ is four momentum. When a Z boson is produced in a

collision and then decays into two opposite charge leptons (l^+l^- , of same flavour), then by conservation of four momentum we get, $p_Z^\mu = p_{l^+}^\mu + p_{l^-}^\mu \implies p_Z^2 = (p_{l^+} + p_{l^-})^2 = M_Z^2$. Thus, the quantity defined by

$$m_{ll} = \sqrt{(p_{l^+} + p_{l^-})^2} \quad (4.6)$$

for pairs of opposite charge leptons of same flavour coming from one collision event, can be very useful for determining whether the pair has been originated from a Z boson or in fact any particle which can decay into opposite charge dilepton final state.

4.1.2 Tools and Methodology

The data collected from collider experiments is stored as particle identity and its four momentum. To identify particles coming from the same event, event reconstruction algorithms are used [54]. For new physics searches, these events are simulated by monte carlo methods using various softwares. Such simulations are useful for giving predictions of new physics.

Lagrangian of new particles is written along with SM Lagrangian in `FeyRules` [55] to generate UFO files, which contain all the interaction vertices from the Lagrangian. This UFO file is then imported in `Madgraph` [56] which simulates large number (N_{seed}) of pp collisions for a specified final state and computes the production cross section (σ'_{sg}). The output of `Madgraph` is a Les Houches Event (LHE)[57] file and events are written as particles, their masses and their four momenta.

Only the information about particle kinematics is not sufficient. Not all the particles produced in collisions are detected due to detector restriction and sensitivity. Also, the final state particles are fundamental particles, which means final state in LHE files can have free quarks. As we discussed in [section 2.1](#), quarks exist only in colorless bound states of baryons or mesons. The free quarks produced in collisions give rise to plethora of other hadrons which lie very close to each other in a narrow cone known as a jet. Hadronization of free quarks in final state along with imposition of detection and event selection criteria is done by `PYTHIA8` [58].

`PYTHIA` reads the LHE file event by event, and constructs jets by various jet construction algorithms. These ‘showered’ events are then scanned particle by particle to check for the possibility of their detection and to select only the desired events (N_{sg}). The final production

cross section is given by

$$\sigma_{sg} = \sigma'_{sg} \frac{N_{sg}}{N_{seed}} \quad (4.7)$$

Similar procedure with same cuts and even selection criteria is performed on some dominant SM process like $pp \rightarrow t\bar{t}$, $pp \rightarrow W^+W^-$, $pp \rightarrow ZZ$ $pp \rightarrow l^+l^-$, etc. The net scattering cross from SM background for the chosen final state is then sum of all scaled production cross sections from SM and is denoted by σ_{bg} . Significance of a signal is defined as

$$\frac{\sigma_{sg}}{\sqrt{\sigma_{bg} + \sigma_{sg}}} \sqrt{L} \quad (4.8)$$

5-sigma significance is considered as a confirmation of a discovery.

4.2 Collider search of SDFDM

The model in the present form is allowed by DM constraints in a large region of DM mass (hundreds of GeV to TeV) generically for small splitting between DM with the heavier component to be aided co-annihilation. However, this still necessitates to have a small mixing angle (between doublet and singlet) to kill the Z-mediated direct search channel. Collider signatures do not seem to be a function of the small mixing and therefore will remain unaffected by the smallness of the angle. Therefore the model can have an early detection at LHC if the mixing angle is very tiny, while direct search will win over collider searches for comparatively larger values of the mixing. After the relic density and direct search constraints, we investigate the possibility of detection of such dark matter model in LHC experiments.

This model contains two unstable particles, a charged lepton (ψ^\pm) and a neutral particle (ψ_2) with masses of order 10^2 GeV. The final product of the decay of both unstable particles contain a neutral and stable DM particle ψ_1 which will escape the detector. This will be seen as missing energy signature in collider. But the interactions of DM $\psi_{1,2}$ involve $\sin\theta$ which are suppressed under the constraint from direct detection $\sin\theta < 0.06$ [Figure 3.10](#). On the other hand, the charged fermion ψ^\pm has nothing to do with the mixing angle and its interactions with Z boson and photon are independent of θ ([Equation 2.19](#)). Thus, ψ^\pm production in the collider experiments through γ and Z mediated Drell-Yan like process depends only on the mass of charged lepton and is independent of $\sin\theta$.

Depending on ΔM , the charged fermions decay further either via two body decay ($\Delta M > M_W$) with on-shell W^\pm boson or via three body decay ($\Delta M < M_W$) with off-shell W^\pm boson into hadronic or leptonic final states of W^\pm boson decay and stable neutral DM ψ_1 . Similarly for ψ_2 with Z boson replacing W^\pm . (Figure 3.5). Both W^\pm and Z bosons can decay into final states containing quark antiquark pair (hadronic decay) which appear as jets in the detector. W^\pm can decay into a lepton and a neutrino while the Z boson decays into opposite charged dileptons of same flavours (leptonic decay).

There are four possibilities of production of particles in dark sector from pp collision, $pp \rightarrow \psi^\pm\psi_1$, $pp \rightarrow \psi^+\psi^-$, $pp \rightarrow \psi^\pm\psi_2$ and $pp \rightarrow \psi_2\psi_2$. All these processes are produced via photon or vector boson mediator. Although, production of $\psi^+\psi^-$ is the only process among these, which is independent of $\sin\theta$. Other processes can contribute significantly and thus will be used for further analysis. Depending upon the subsequent decays of particles, following final states are possible for each process.

(A) $pp \rightarrow \psi^\pm\psi_1, \psi^\pm \rightarrow W^\pm\psi_1$

- (a) Hadronic decay of W^\pm : 2 jets + missing energy
- (b) Leptonic decay of W^\pm : a lepton + missing energy

(B) $pp \rightarrow \psi^+\psi^-, \psi^\pm \rightarrow W^\pm\psi_1$

- (a) Both W^\pm decay hadronically: 4 jets + missing energy.
- (b) One decays hadronically and other leptonically: 2 jets + a lepton + missing energy.
- (c) Both decay leptonically: opposite di-lepton signal + missing energy.

(C) $pp \rightarrow \psi^\pm\psi_2, \psi^\pm \rightarrow W^\pm\psi_1, \psi_2 \rightarrow Z\psi_1$

- (a) Both W^\pm and Z boson decay hadronically : 4 jets + missing energy
- (b) Hadronic decay of W^\pm and leptonic decay of Z boson : 2 jets + opposite sign di-lepton of same flavor + missing energy
- (c) Hadronic decay of Z and leptonic decay of W^\pm boson : 2 jets + a lepton + missing energy
- (d) Both W^\pm and Z boson decay leptonically : 3 leptons + missing energy

(D) $pp \rightarrow \psi_2\psi_2, \psi_2 \rightarrow Z\psi_1$

- (a) Both Z bosons decay hadronically : 4 jets + missing energy
- (b) Hadronic decay of one Z and leptonic decay the other : 2 jets + opposite sign di-lepton of same flavor + missing energy
- (c) Both Z bosons decay leptonically : 2 pairs of opposite sign di-leptons + missing energy

To look for such signals at LHC, it is important to reduce the SM background. The dominant decay of W and Z boson is into hadronic final states of 2 jets compared to leptonic final state of electrons and muons. Thus, we will only look for the leptonic final states as these are clean signals to detect at LHC (see Figure 4.2). Thus our events are leptonic final states with number of leptons from one to four (Figure 1.3).

From Figure 3.4, it is clear that the direct search experiments restrict $\sin \theta$ to be less than 0.04 for any dark matter mass. As explained in chapter 3, for small $\sin \theta$ the relic density is satisfied either in resonance region or due to the co-annihilation. Figure 3.8a suggests that for lowering the relic density to satisfy the observed data, ΔM must be small (~ 10 GeV). This suggests that the W/Z boson decays will be off-shell.

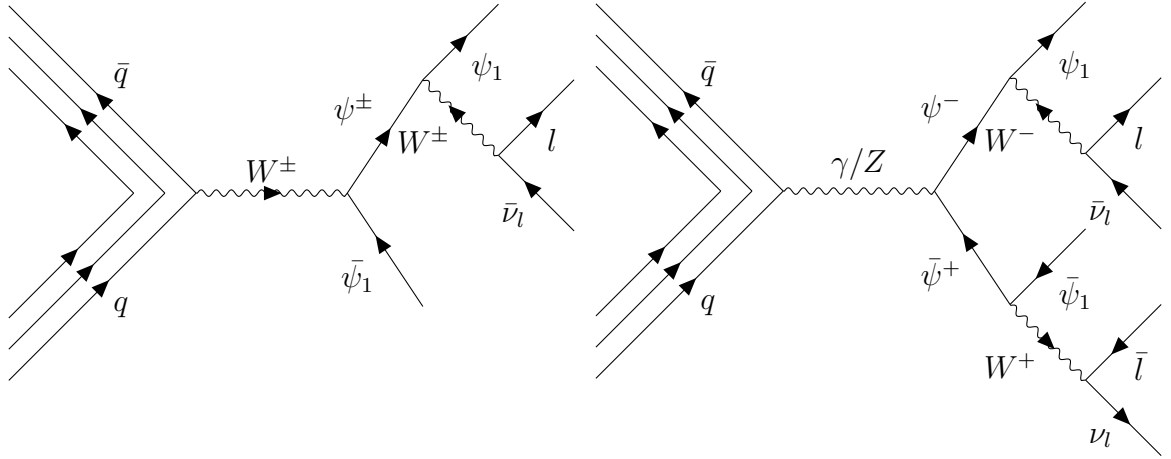
We now proceed to analyze the LHC phenomenology for four benchmark points which satisfies the relic density criteria and direct search constraints.

Name	M_{ψ_1} (GeV)	ΔM (GeV)	$\sin \theta$	Ωh^2	$\ln \sigma_{SI}/cm^2$
BP1	111	9	0.03	0.1150	-46.199
BP2	143	10	0.04	0.1177	-45.623
BP3	288	11	0.03	0.1167	-46.120
BP4	85	8	0.02	0.1165	-46.833

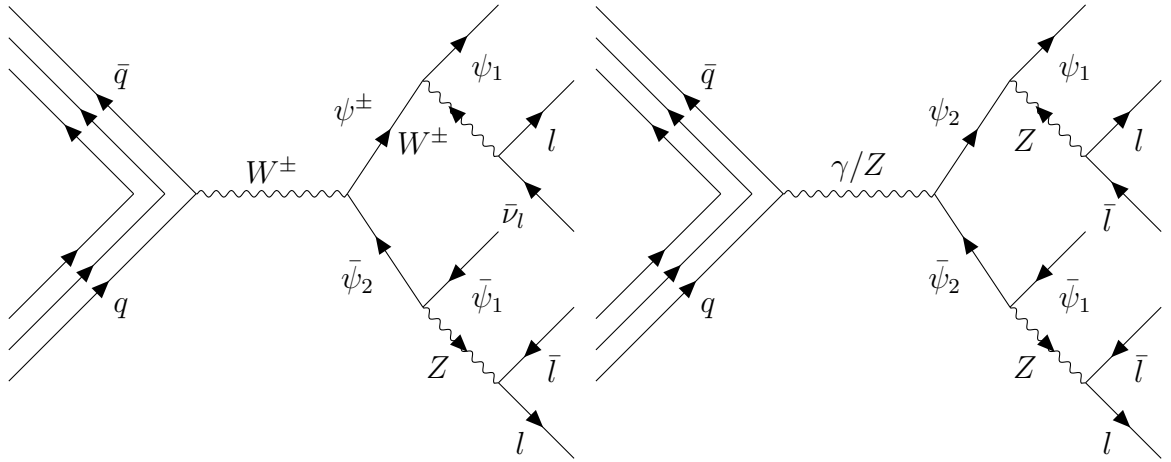
Table 4.1: Benchmark Points

4.3 Results and Discussion for Collider Searches of SDFDM Model

We have implemented this model in MadGraph using FeynRules and generated the parton level events using CTEQ6L [59] parton distribution function for $\sqrt{s} = 14$ TeV. These events



(a) Final state is single lepton and missing energy (b) Final state is opposite dilepton and missing energy



(c) Final state is 3 leptons and missing energy (d) Final state is 4 leptons and missing energy

Figure 4.2: Feynman diagrams showing leptonic final state events for SDFDM model in collider searches.

were feed into PYTHIA8 for showering and hadronization. To simulate the LHC detector we have used following identification criteria:

1. Leptons ($l = e, \mu$): Minimum transverse momentum was set to 7 GeV, lower than the usual 20 GeV, as our interest is in soft lepton region. Leptons were restricted to the central region of detector by $|\eta| < 2.5$. Two leptons are identified distinctly if the angular separation (Equation 4.3) $R_{ll} \geq 0.2$. Lepton-jet separation must be $R_{lj} \geq 0.4$ to resolve lepton from jets. As τ leptons have very short lifetime, they are difficult to observe in electromagnetic

calorimeters or muon detectors, and hence are not considered in lepton category in collider physics.

2. Jets:

We have used `SlowJet`, a function in `PYTHIA8` for jet construction from hadrons. Jets were identified using anti-kT algorithm [60]. The jet is defined by the clustered hadrons within the cone of angular separation $R_{cone} \leq 0.4$. Jets were also required to be in the central region of detector, $|\eta| < 2.5$. For registering jet, all components are required to have minimum transverse momentum of 20 GeV ($p_T \geq 20$ GeV). Invisible components were excluded from the jets if they lie within the jetcone and proper masses of all particles were used in `SlowJet` function.

3. Unclustered Objects:

All visible final state objects which are not identified leptons and are separated from jets are considered as unclustered objects. This includes low p_T and $2.5 < |\eta| < 5$ leptons who leave their presence in the detector. Unclustered objects are required to be well separated from jets by imposing $R_{uj} \geq 0.4$. Since the unclustered objects are visible, their contribution is considered in the calculation of missing transverse energy (Equation 4.4).

The distributions for three observables:

1. Missing transverse energy (E_T^{miss})
2. Lepton transverse momentum (p_T)
3. Dilepton invariant mass (m_{ll}), for all possible combinations of opposite charge same flavor leptons.

for BP1 are plotted using the mentioned minimum detection criteria (Figure 4.3). The distributions are similar for other benchmark points section B.2, as the selected benchmark points, which are allowed by relic density and direct detection, lie very close to each other in terms of all three parameters. We have also plotted the distributions of same observables for five SM background processes (Table 4.2) which contribute dominantly for multilepton final state. The production cross-sections for these processes were calculated by taking the next to leading order (NLO) contributions.

Process	σ (pb)
$pp \rightarrow l^+l^-$ (Drell-Yan)	879.19
$pp \rightarrow t\bar{t}$	814.64
$pp \rightarrow W^+W^-$	100.48
$pp \rightarrow ZZ$	14.01
$pp \rightarrow W^+W^-Z$	0.15

Table 4.2: SM background

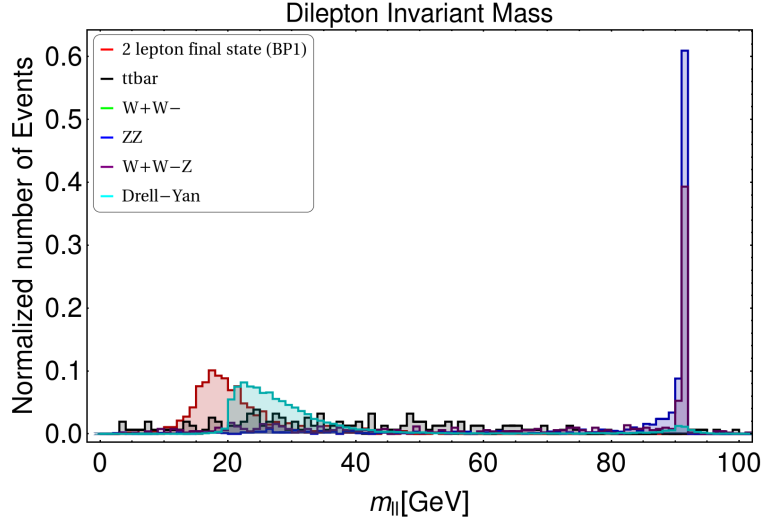
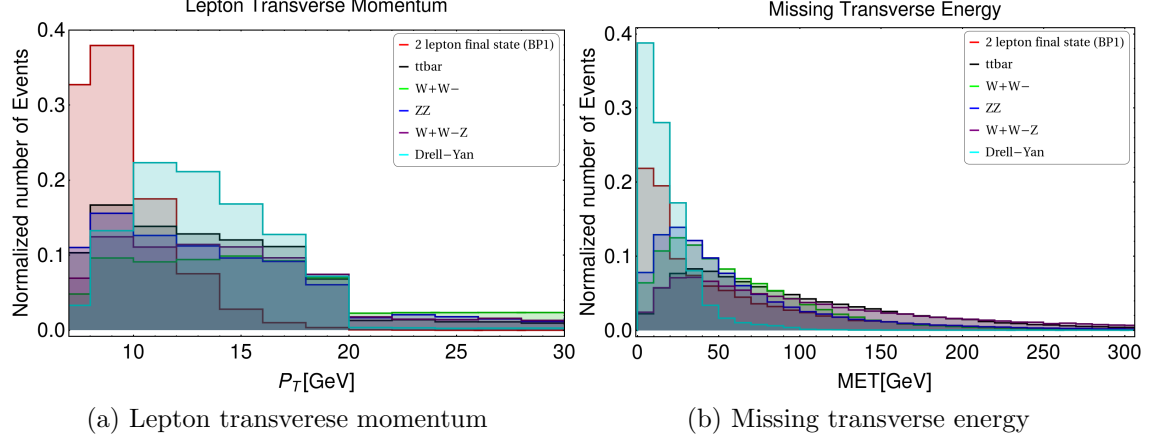


Figure 4.3: Distributions for a benchmark point BP1 given by $M_{\psi_1} = 111$ GeV, $\Delta M = 9$ GeV and $\sin\theta = 0.03$. The beam center of mass energy is 14 TeV and the distributions are for opposite dilepton final state. Final leptons are selected with $p_T > 7$ GeV, $\eta < 2.5$, $R_{ll} > 0.2$, $R_{lj} > 0.4$ and $R_{jj} > 0.4$

The missing transverse energy distribution for DM is completely suppressed throughout the region (Figure 4.3b). In Drell-Yan processes, the final state has just leptons, which are visible and thus have almost no missing transverse energy. The only contribution is from unclustered objects. Hence, the small MET region has heavy contribution from Drell-Yan processes. In the region $MET > 50$ GeV, DM signal is very low. This is because of the small mass splitting ΔM which causes off-shell vector boson production making it a three body decay. The momentum carried away by the invisible component ψ_1 in the transverse plane is very small because of small difference between mass of ψ_1 and mass of $\psi^\pm(\psi_2)$. On the other hand, the dominant SM backgrounds of $pp \rightarrow W^+W^-$ and $pp \rightarrow ZZ$ have on shell vector bosons, decaying into two particles and the mass difference between initial and final particles is around 90 GeV.

The off-shell nature of decay also explains the distribution of transverse momentum of leptons for DM signals(Figure 4.3a) by the same reasoning as above. On the other hand, leptons from on-shell decays of vector bosons from SM process have very large momenta. For Drell-Yan processes, the leptons are produced directly from pp collision and thus have very high p_T . The three body decay in the DM signal, as explained earlier, will cause the leptons to have very small momentum in transverse plane dominating the p_T distribution over SM background in the soft lepton region (7-10 GeV).

Although the small ΔM makes the DM signal difficult to detect for large missing energies cuts for event selection, it comes to the rescue for dilepton invariant mass cut of Z window. Since the SM background coming from $pp \rightarrow W^+W^-Z$ and $pp \rightarrow ZZ$ processes, which dominate in the low missing energy region, are almost killed by di-lepton invariant mass cut (due to on-shell Z boson) demanding the value to lie outside Z mass window (75-105 GeV) (Figure 4.3c). On the other hand, the DM signal is unaffected by this cut as Z boson is off-shell.

4.3.1 Event selection

Along with minimum detection criteria, events are selected using following cuts:

1. Jets:

Event final state is purely leptonic, we have put a jet veto for event selection.

2. Lepton transverse momentum (p_T):

Lepton transverse momentum distribution is peaked in soft lepton region. Thus we have selected final state leptons with $7 \text{ GeV} \leq p_T \leq 20 \text{ GeV}$

3. Dilepton invariant mass (m_{ll}):

As explained earlier, m_{ll} should lie outside the Z mass window, $75 \text{ GeV} \not\leq m_{ll} \not\leq 105 \text{ GeV}$

The production cross section for the four benchmark points from **MadGraph** (σ'_{sg}) is given in [Table 4.3](#). It is then rescaled (σ_{sg}) using N_{sg} and N_{seed} , as explain in [subsection 4.1.2](#), for 2, 3, and 4 lepton final state. We are skipping the single lepton final state analysis as the background for that signal is huge as a lot of contributions come from other than mentioned SM background processes, which makes the single lepton channel noisy. N_{eff} is then calculated for 1000 fb^{-1} luminosity by $N_{eff} = \sigma_{sg}^{tot} \times L$. σ_{sg}^{tot} here is the total rescaled production cross section for that particular final states with more number of leptons contributing to the signal containing fewer leptons. [Table 4.3](#) and [Table 4.4](#) show the effective number of events for both SDFDM benchmark points and SM background.

Name	σ'_{2l} (pb)	σ'_{3l} (pb)	σ'_{4l} (pb)	N_{eff} (2l)	N_{eff} (3l)	N_{eff} (4l)
BP1	0.0675	0.0880	0.0090	255	13	< 1
BP2	0.0281	0.0357	0.0036	289	23	< 1
BP3	0.0023	0.0028	0.0003	7	< 1	< 1
BP4	0.1713	0.0810	0.0030	384	8	< 1

Table 4.3: Effective number of events for multi-lepton final states. $L = 1000 \text{ fb}^{-1}$

Name	N_{eff} (2l)	N_{eff} (3l)	N_{eff} (4l)
$pp \rightarrow t\bar{t}$	48878	< 1	< 1
$pp \rightarrow W^+W^-$	62298	1005	< 1
$pp \rightarrow ZZ$	3923	140	< 1
$pp \rightarrow W^+W^-Z$	33	< 1	< 1
Drell-Yan	$\sim 10^8$	35168	8792

Table 4.4: SM background for multi-lepton final states. $L = 1000 \text{ fb}^{-1}$

The DM signal is completely shadowed by the strong SM background even for Luminosity as high as 1000fb^{-1} . The lack of large missing energies due to small ΔM can't kill the most

dominant channel of Drell-Yan processes. Also, since the Z boson is not produced on-shell in Drell-Yan, it survives the dilepton invariant mass cut. The significance (Equation 4.8) of signal for all benchmark points doesn't reach the 5-sigma confidence (Figure 4.4) even for Luminosity as high as 10^6 , which is nowhere near the future LHC plan.

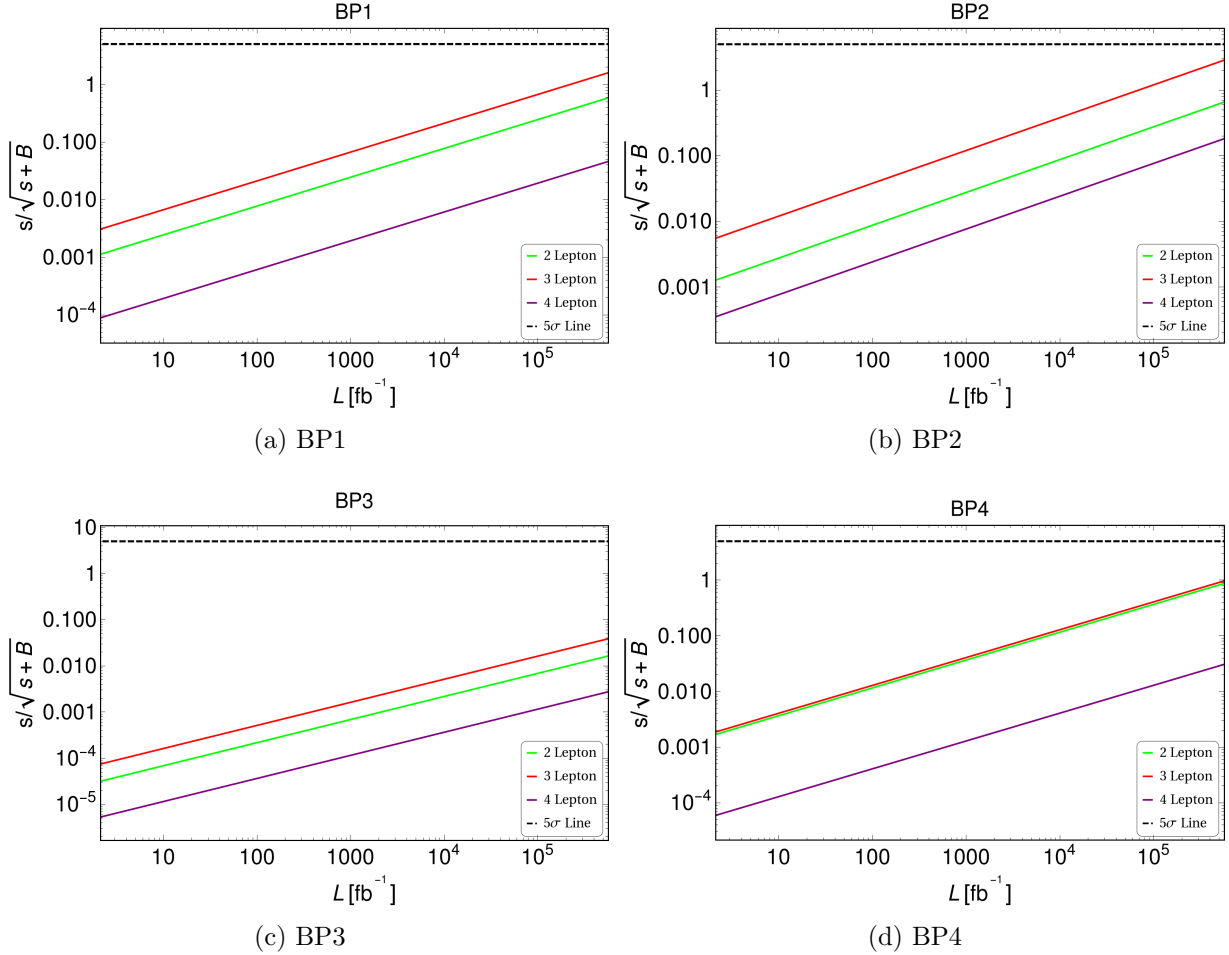


Figure 4.4: Significance plots for benchmark points

Although this model is difficult to detect in future collider search experiments via counting the leptonic final state events, there is another way in which the signature of this model can be tested at LHC. Since the $\psi^\pm \rightarrow \psi_1, l, \nu_l$ is heavily suppressed due to small $\sin\theta$, the decay of the charged particle is delayed. This can be seen as a displaced charged vertex signal in collider as the charged lepton travels for significant distance through the detector before decaying. Γ , is the decay width of ψ^\pm decaying into lepton via three body decay, which is

given by [61]

$$\Gamma_{\psi^\pm \rightarrow \psi_1 l^\pm \nu_l} = \frac{G_F^2 \sin^2 \theta}{24\pi^3} M_2^5 I\left(\frac{M_1}{M_2}, \frac{m_l}{M_2}\right) \quad (4.9)$$

$$I(a, b) = \frac{1}{4} \lambda(a, b) F_1(a, b) - 3F_2(a, b) + 3F_3(a, b) \quad (4.10)$$

$$\lambda(a, b) = \sqrt{1 + a^4 + b^4 - 2a^2 - 2b^2 - 2a^2 b^2} \quad (4.11)$$

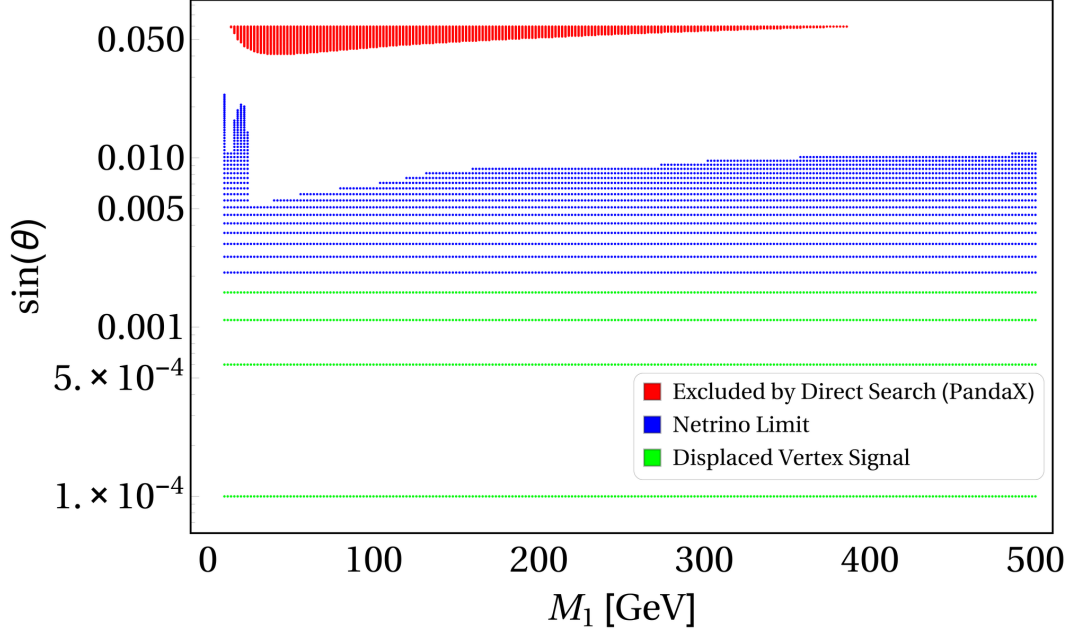
$$F_1(a, b) = 1 - 2a^5 + a^6 - 7b^2 - 7b^4 + b^6 + 10a^3(-2 + b^2) - 7a^4(1 + b^2) + a^2(-7 + 12b^2 - 7b^4) + 2a(-1 + 5b^2 + 2b^4) \quad (4.12)$$

$$F_2(a, b) = (-1 + a - a^3 + a^4) b^4 \log 2a + (-2a^5 + b^4 - ab^4 + a^4(-2 + b^4) - a^3(2 - 4b^2 + b^4)) \log 2a \quad (4.13)$$

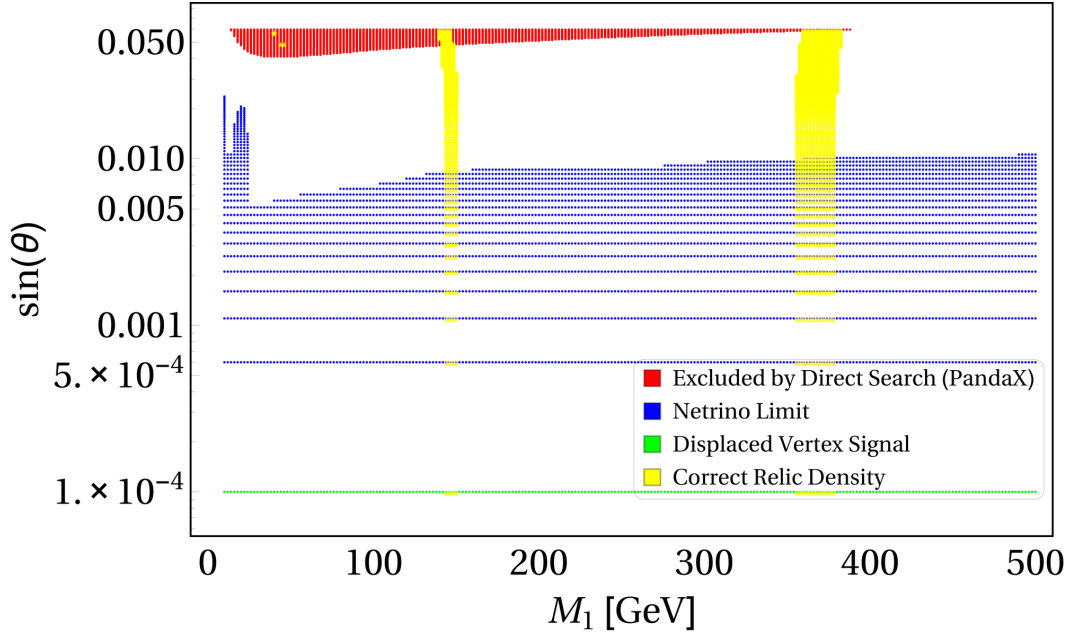
$$F_3(a, b) = -(-1 + a^2)(1 - a + a^2) b^4 \log b^2 - (2a^5 - b^4 + ab^4 - a^4(-2 + b^4) + a^3(2 - 4b^2 + b^4)) \times \log(1 + a^2 - b^2 - \lambda(a, b)) + (-1 + a^2)(1 - a + a^2) b^4 \times \log(1 + a^4 - b^2 - \lambda(a, b) + a^2(-2 - b^2 + \lambda(a, b))) \quad (4.14)$$

where G_F is Fermi coupling constant, is used to measure displaced vertex signal. In order see such signal in collider experiments, the decay length $L = \frac{1}{\Gamma}$ must be of the order of detector length ($\sim 1 - 10$ cm) [53].

In Figure 4.5, we have shown the parameter space (green region), where such signal is possible. The decay length of this region is of greater than a centimetre. The blue region in the graph has spin independent cross section with nucleon (σ_{SI}) comparable to neutrinos. Such region can't be probed in direct detection experiments due to tremendous noise from atmospheric neutrinos colliding with nucleons. Comparing Figure 4.5a and Figure 4.5b in, we can see that the decay width increases (and thus decay length decreases) for large mass splitting leaving a smaller region of the parameter space accessible for displaced vertex signal. Also, the future direct detection region and visible displaced vertex signal region are mutually exclusively.



(a) $\Delta M = 5$ GeV



(b) $\Delta M = 10$ GeV

Figure 4.5: $\sin \theta$ vs. M_1 plots for fixed ΔM , $\Delta M = 5$ GeV (left) and $\Delta M = 10$ GeV (right). Red region indicates the bounds from PandaX experiments [23]. Blue region of the parameter space has direct search cross section less than neutrino direct search cross sections. These points will never be detected in direct search experiments. The green points can be seen as displaced charged vertex in the LHC experiments ($\Gamma^{-1} > 1\text{cm}$). Yellow points satisfy the relic density constraint ($0.1133 \leq \Omega h^2 \leq 0.1189$)[13].

Chapter 5

Conclusions and Outlook

We have analyzed the parameter space of vector-like singlet doublet fermionic dark matter (SDFDM) model in the light of relic density criteria, recent direct detection experiments and possible collider search at LHC. Significant region of the parameter space is still allowed even after putting former two constraints (Figure 3.10). Among the leftover parameter space, we analyzed four benchmark points (Table 4.1) fairly spread over all three parameters for collider search signal of multi-lepton final states consisting 2, 3, and 4 leptons. Vector-like SDFDM model detection for mentioned final state requires extremely high luminosity ($\sim 10^6 \text{ fb}^{-1}$) to achieve 5σ significance as the SM background for the same final states is extremely high and can't be cut down due to the absence of large missing energies in DM signal (Figure B.1). Since the proposed future LHC runs can go upto luminosity 3000 fb^{-1} [52], the signatures of this model are nearly impossible to see at LHC. Instead, a significant region of parameter space is accessible in LHC experiments for displaced vertex signal of charged lepton (Figure 4.5) and is exclusively separated from the upper limit of future direct detection experiments constrained by neutrino noise.

In the future aspects of this work, we propose to analyze the same event signal at LHC with an extension of SM scalar triplet to the vector-like SDFDM model [62]. Such addition of scalar triplet introduces a majorana mass splitting to the neutral particles ψ_1, ψ_2 (Appendix C). This changes their interaction with Z boson shown in Equation 2.16 by introducing a particle splitting. Thus, such model becomes extremely difficult to observe in direct detection experiments as the DM, which is the low mass component among the

split ψ_1 , has to change to heavier particle after collision with nucleons via Z interaction. It decreases the σ_{SI} significantly allowing the parameter space to become accessible even for large $\sin\theta$. Since, the splitting can be tuned to be very small, it doesn't affect the thermal evolution of the particle leaving no change in the relic density criteria. But importantly, no restriction on mixing angle allows us to explore the parameter space beyond co-annihilation region while still satisfying the relic density. Access to large $\sin\theta$ and ΔM allows the charged leptons to decay via two body decay, thus giving large missing transverse energy signals as discussed in [section 4.3](#). Putting a large missing energy cut on event selection will reduce the SM background while keeping the new physics signal significant. We propose to analyze this extended model under the mentioned event selection to see whether its signals are significantly visible for luminosity proposed in future LHC runs.

Appendix A

Weinberg-Salam Model

This chapter reviews the electroweak interaction theory in SM and is heavily based upon [43, ch. 15]

A.1 Electroweak Theory

The idea of gauge theory came from Quantum Electrodynamics (QED). The Lagrangian of a fermion interacting with each other via electromagnetic force is given by

$$\mathcal{L}_{QED} = i\bar{\psi}\gamma^\mu\partial_\mu\psi - m_\psi\bar{\psi}\psi + e\bar{\psi}\gamma^\mu A_\mu\psi - \frac{1}{4}F^{\mu\nu}F_{\mu\nu}, \quad F_{\mu\nu} = \partial_\mu A_\nu - \partial_\nu A_\mu \quad (\text{A.1})$$

First, note that in the electromagnetic Lagrangian, the last term is invariant under a gauge transformation

$$A_\mu \rightarrow A_\mu + \frac{1}{e}\partial_\mu\lambda(x) \quad (\text{A.2})$$

where lambda is an arbitrary scalar function of space-time. This means the electrodynamics should always remain invariant under the gauge transformation of vector field A_μ . But the third term in (A.1) shifts such that there is an additional derivative term similar to the first kinetic term. To keep the Lagrangian invariant under such gauge transformation we must transform ψ and modify the Lagrangian so that this additional term is absorbed. This can

be done by transforming the fermion field simultaneously as

$$\psi(x) \rightarrow e^{i\lambda(x)}\psi(x) \quad \bar{\psi}(x) \rightarrow e^{-i\lambda(x)}\bar{\psi}(x) \quad (\text{A.3})$$

so that

$$\partial_\mu\psi(x) \rightarrow i\partial_\mu\lambda(x)e^{i\lambda(x)}\psi(x) + e^{i\lambda(x)}\partial_\mu\psi(x) \quad (\text{A.4})$$

The first term here can be used to cancel out the additional term that bothered us. We can do this by rewriting (A.1) as

$$\mathcal{L}_{QED} = i\bar{\psi}\gamma^\mu(\partial_\mu - ieA_\mu)\psi - m_\psi\bar{\psi}\psi - \frac{1}{4}F^{\mu\nu}F_{\mu\nu} \quad (\text{A.5})$$

If we redefine the derivative term as

$$D_\mu = \partial_\mu - ieA_\mu \quad (\text{A.6})$$

then it transforms under the gauge transformation similar to (A.3) making the kinetic term invariant.

$$D_\mu\psi \rightarrow e^{i\lambda(x)}D_\mu\psi(x) \quad (\text{A.7})$$

If one thinks in the opposite way and starts from demanding that local phase transformation of fermion field to be the symmetry of Lagrangian, i.e. (A.3), which is a $U(1)$ gauge theory, then entire QED emerges out of it as one needs to introduce a vector field A_μ and its kinetic term.

This was in fact the basic motivation behind explaining all forces by gauge theories. The generalization of this mechanism to weak force introduces another gauge symmetry $SU(2)$. The covariant derivative term for this unified $SU_L(2) \otimes U_Y(1)$ is then given by

$$D_\mu = \partial_\mu + ig\frac{\sigma^a}{2}W_\mu^a + ig'\frac{Y}{2}B^\mu \quad (\text{A.8})$$

where W^a are the generators of $SU_L(2)$ with transformation

$$W_\mu^a \rightarrow W_\mu^a - \frac{1}{g}\partial_\mu\lambda^a(x) - \epsilon^{abc}\lambda^b(x)W_\mu^c \quad (\text{A.9})$$

and B^μ is the generator of $U_Y(1)$. Since the $SU(2)$ group is non-abelian, the generators don't commute and it has an important consequence, the kinetic term of gauge bosons is changed

to accommodate the non-commuting part as

$$\mathcal{L}_{SU(2)} = -\frac{1}{4}\mathbf{W}_{\mu\nu} \cdot \mathbf{W}^{\mu\nu} \quad W_{\mu\nu}^a = \partial_\mu W_\nu^a - \partial_\nu W_\mu^a - g\epsilon^{abc}W_\mu^b W_\nu^c \quad (\text{A.10})$$

Also, note that the parity violation in weak force prevents us to write explicit fermion mass term $\bar{\psi}\psi$ as mentioned in §2.1.

A.2 Spontaneous Symmetry Breaking and Particle Masses

To solve the problem of massless fermions and gauge bosons, we introduce complex scalar field with hypercharge $Y = 1$, $H = \begin{pmatrix} H^+ \\ H^0 \end{pmatrix}$, which is doublet under $SU_L(2)$. The renormalizable Lagrangian for such field is given by

$$\mathcal{L} = (D^\mu H)^\dagger (D_\mu H) - \mu^2 H^\dagger H - \lambda (H^\dagger H)^2 \quad (\text{A.11})$$

For $\mu^2 < 0$ this potential has a nonzero ground state. By choosing the vacuum expectation value as $\langle H \rangle = \frac{1}{\sqrt{2}} \begin{pmatrix} 0 \\ v \end{pmatrix}$ and expanding the field about it as

$$H = \frac{1}{\sqrt{2}} \begin{pmatrix} 0 \\ v + h \end{pmatrix} \quad (\text{A.12})$$

where h is the scalar field expanded about the vacuum. With this we explicitly rewrite the (A.11) by using (A.8) with $Y = 1$ and keep the terms without h which are two particle terms.

$$\begin{aligned} \left| \left(ig \frac{\sigma^a}{2} W_\mu^a + ig' \frac{1}{2} B^\mu \right) H \right|^2 &= \frac{1}{8} \left| \begin{pmatrix} gW_\mu^3 + g'B_\mu & g(W_\mu^1 - iW_\mu^2) \\ g(W_\mu^1 + iW_\mu^2) & -gW_\mu^3 + g'B_\mu \end{pmatrix} \begin{pmatrix} 0 \\ v \end{pmatrix} \right|^2 \\ &= \frac{1}{8} v^2 g^2 [(W_\mu^1)^2 + (W_\mu^2)^2] + \frac{1}{8} v^2 (g'B_\mu - gW_\mu^3)(g'B^\mu - gW^{3\mu}) \\ &= \left(\frac{1}{2} vg \right)^2 W_\mu^+ W^{-\mu} + \frac{1}{8} v^2 (W_\mu^3, B_\mu) \begin{pmatrix} g^2 & -gg' \\ -gg' & g'^2 \end{pmatrix} \begin{pmatrix} W^{3\mu} \\ B^\mu \end{pmatrix} \end{aligned}$$

where $W^\pm = (W_\mu^1 \mp iW_\mu^2)/\sqrt{2}$. The first term in the last line gives the mass of charged vector boson as $M_W = gv/2$ while the second term is not diagonalized in the mass basis. The eigenvalues of the matrix are $M_A = 0$ and $M_Z = \frac{1}{2}v\sqrt{g^2 + g'^2}$, which are the masses of photon and Z boson respectively, with eigenstates

$$A_\mu = \cos \theta_W B_\mu + \sin \theta_W W_\mu^3 \quad (\text{A.13})$$

$$Z_\mu = -\sin \theta_W B_\mu + \cos \theta_W W_\mu^3 \quad (\text{A.14})$$

$$\tan \theta_W = \frac{g}{g'} \quad (\text{A.15})$$

The masses of fermions are also generated in the similar manner. The Higgs field being a $SU_L(2)$ doublet, interacts with the fermions via Yukawa interaction given by

$$\mathcal{L}_{Yukawa} = -G_e \left[(\bar{\nu}_e, \bar{e})_L \begin{pmatrix} H^+ \\ H^0 \end{pmatrix} e_R + \bar{e}_R (H^-, H^0) \begin{pmatrix} \nu_e \\ e \end{pmatrix}_L \right] \quad (\text{A.16})$$

Since the e_R is singlet under $SU_L(2)$, it remains invariant under but the first two doublets transform such that they nullify each others effects and remain invariant. Again expanding (A.16) with (A.12) and neglecting the terms with h ,

$$\mathcal{L}_{Yukawa-Mass} = -\frac{G_e}{\sqrt{2}}v(\bar{e}_L e_R + \bar{e}_R e_L) = -\frac{G_e}{\sqrt{2}}v\bar{e}e \quad (\text{A.17})$$

which is the mass term for electron with $m_e = \frac{G_e}{\sqrt{2}}v$. There is a slight difference for giving mass to quark sector as there we need to give mass to both the components of doublet, unlike leptons. For that we will use the fact that $\tilde{H} = i\sigma_2 H^*$ transforms similar to H under $SU_L(2)$. With this we will write the Yukawa interaction with quarks and expand it using (A.12)

$$\mathcal{L}_{Yukawa} = -G_d(\bar{u}, \bar{d})_L \begin{pmatrix} H^+ \\ H^0 \end{pmatrix} d_R - G_u(\bar{u}, \bar{d})_L \begin{pmatrix} -\tilde{H}^0 \\ H^- \end{pmatrix} u_R + \text{hermitian conjugate} \quad (\text{A.18})$$

$$= -m_d \bar{d}d - m_u \bar{u}u \dots \text{ keeping only the mass terms} \quad (\text{A.19})$$

A.3 The Final Lagrangian

As explained above, the electroweak theory with additional scalar doublet along with SSB mechanism explains particle masses and gives correct interactions. It is thus useful to summarize the final Lagrangian as we have used it for constructing DM in BSM scenario.

$$\mathcal{L} = -1\frac{1}{4}\mathbf{W}_{\mu\nu} \cdot \mathbf{W}^{\mu\nu} - \frac{1}{4}B_{\mu\nu}B^{\mu\nu} \quad \text{Kinetic terms for vector bosons} \quad (\text{A.20})$$

$$+ i\bar{L}\gamma^\mu \left(\partial_\mu + ig\frac{\sigma^a}{2}W_\mu^a + ig'\frac{Y}{2}B^\mu \right) L \quad \text{Kinetic term for left handed fermions} \quad (\text{A.21})$$

$$+ i\bar{R}\gamma^\mu \left(\partial_\mu + ig'\frac{Y}{2}B^\mu \right) R \quad \text{Kinetic term for right handed fermions} \quad (\text{A.22})$$

$$\left| \left(ig\frac{\sigma^a}{2}W_\mu^a + ig'\frac{1}{2}B^\mu \right) H \right|^2 \quad \text{Kinetic term for Higgs field} \quad (\text{A.23})$$

$$- \mu^2 H^\dagger H - \lambda(H^\dagger H)^2 \quad \text{Higgs potential} \quad (\text{A.24})$$

$$- (G_1\bar{L}HR + G_2\tilde{H}R + \text{h.c}) \quad \text{Lepton and quark couplings to Higgs} \quad (\text{A.25})$$

Appendix B

Additional Data

B.1 MicrOMEGA output of BP1

Dark matter candidate is ' $\tilde{\psi}1$ ' with spin=1/2 mass=1.11E+02

=== MASSES OF HIGGS AND ODD PARTICLES: ===

Higgs masses and widths

h 125.00 3.91E-03

Masses of odd sector Particles:

$\tilde{\psi}1$: MDM = 111.0 || $\tilde{\psi}1$: M ψ ic = 120.0 || $\tilde{\psi}1$: M ψ i2 = 120.0

==== Calculation of relic density =====

Xf=2.63e+01 Omega=1.15e-01

Channels which contribute to 1/(omega) more than 1%.

Relative contributions in % are displayed

15% $\tilde{\psi}2$ $\tilde{\Psi}+$ ->D u

15% $\tilde{\psi}2$ $\tilde{\Psi}+$ ->S c

5% $\tilde{\psi}2$ $\tilde{\Psi}+$ ->E ne

5% $\tilde{\psi}2$ $\tilde{\Psi}1+$ $\rightarrow M$ nm
 5% $\tilde{\psi}2$ $\tilde{\Psi}1+$ $\rightarrow L$ nl
 5% $\tilde{\psi}2$ $\tilde{\Psi}1+$ $\rightarrow B$ t
 3% $\tilde{\psi}2$ $\tilde{\Psi}1+$ $\rightarrow Z$ W+
 3% $\tilde{\psi}1-$ $\tilde{\Psi}1+$ $\rightarrow W+$ W-
 3% $\tilde{\psi}2$ $\tilde{\Psi}12$ $\rightarrow d$ D
 3% $\tilde{\psi}2$ $\tilde{\Psi}12$ $\rightarrow s$ S
 3% $\tilde{\psi}2$ $\tilde{\Psi}12$ $\rightarrow b$ B
 2% $\tilde{\psi}1-$ $\tilde{\Psi}1+$ $\rightarrow u$ U
 2% $\tilde{\psi}1-$ $\tilde{\Psi}1+$ $\rightarrow c$ C
 2% $\tilde{\psi}2$ $\tilde{\Psi}12$ $\rightarrow W+$ W-
 2% $\tilde{\psi}2$ $\tilde{\Psi}12$ $\rightarrow u$ U
 2% $\tilde{\psi}2$ $\tilde{\Psi}12$ $\rightarrow c$ C
 2% $\tilde{\psi}2$ $\tilde{\Psi}1+$ $\rightarrow A$ W+
 2% $\tilde{\psi}1-$ $\tilde{\Psi}1+$ $\rightarrow d$ D
 2% $\tilde{\psi}1-$ $\tilde{\Psi}1+$ $\rightarrow s$ S
 2% $\tilde{\psi}1-$ $\tilde{\Psi}1+$ $\rightarrow b$ B
 1% $\tilde{\psi}2$ $\tilde{\Psi}12$ $\rightarrow Z$ Z
 1% $\tilde{\psi}2$ $\tilde{\Psi}12$ $\rightarrow ne$ Ne
 1% $\tilde{\psi}2$ $\tilde{\Psi}12$ $\rightarrow nm$ Nm
 1% $\tilde{\psi}2$ $\tilde{\Psi}12$ $\rightarrow nl$ Nl
 1% $\tilde{\psi}2$ $\tilde{\Psi}1+$ $\rightarrow W+$ h
 1% $\tilde{\psi}1-$ $\tilde{\Psi}1+$ $\rightarrow e$ E
 1% $\tilde{\psi}1-$ $\tilde{\Psi}1+$ $\rightarrow m$ M
 1% $\tilde{\psi}1-$ $\tilde{\Psi}1+$ $\rightarrow l$ L

==== Calculation of CDM-nucleons amplitudes =====

CDM[antiCDM]-nucleon micrOMEGAs amplitudes for $\tilde{\psi}1$

proton: SI -4.177E-10 [4.134E-10] SD -1.175E-30 [1.175E-30]

neutron: SI 3.834E-09 [-3.838E-09] SD 4.291E-30 [-4.291E-30]

CDM[antiCDM]-nucleon cross sections[pb]:

proton SI 7.499E-11 [7.344E-11] SD 1.780E-51 [1.780E-51]

neutron SI 6.318E-09 [6.333E-09] SD 2.375E-50 [2.375E-50]

B.2 Distributions for all benchmark points

2 Lepton Final State

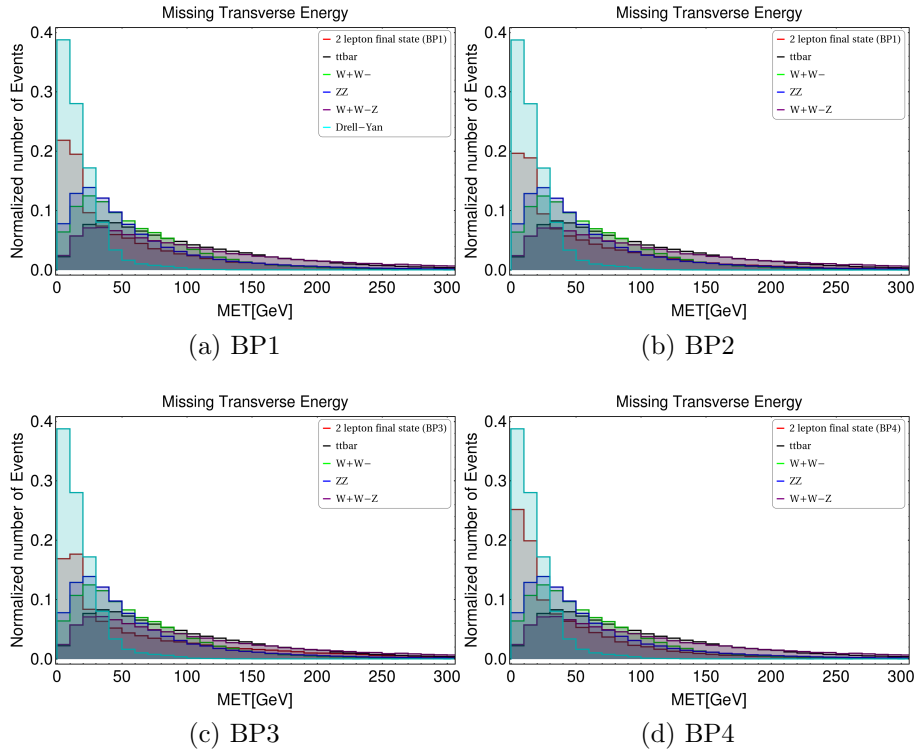


Figure B.1: Missing transverse energy (MET) distributions for all benchmark points

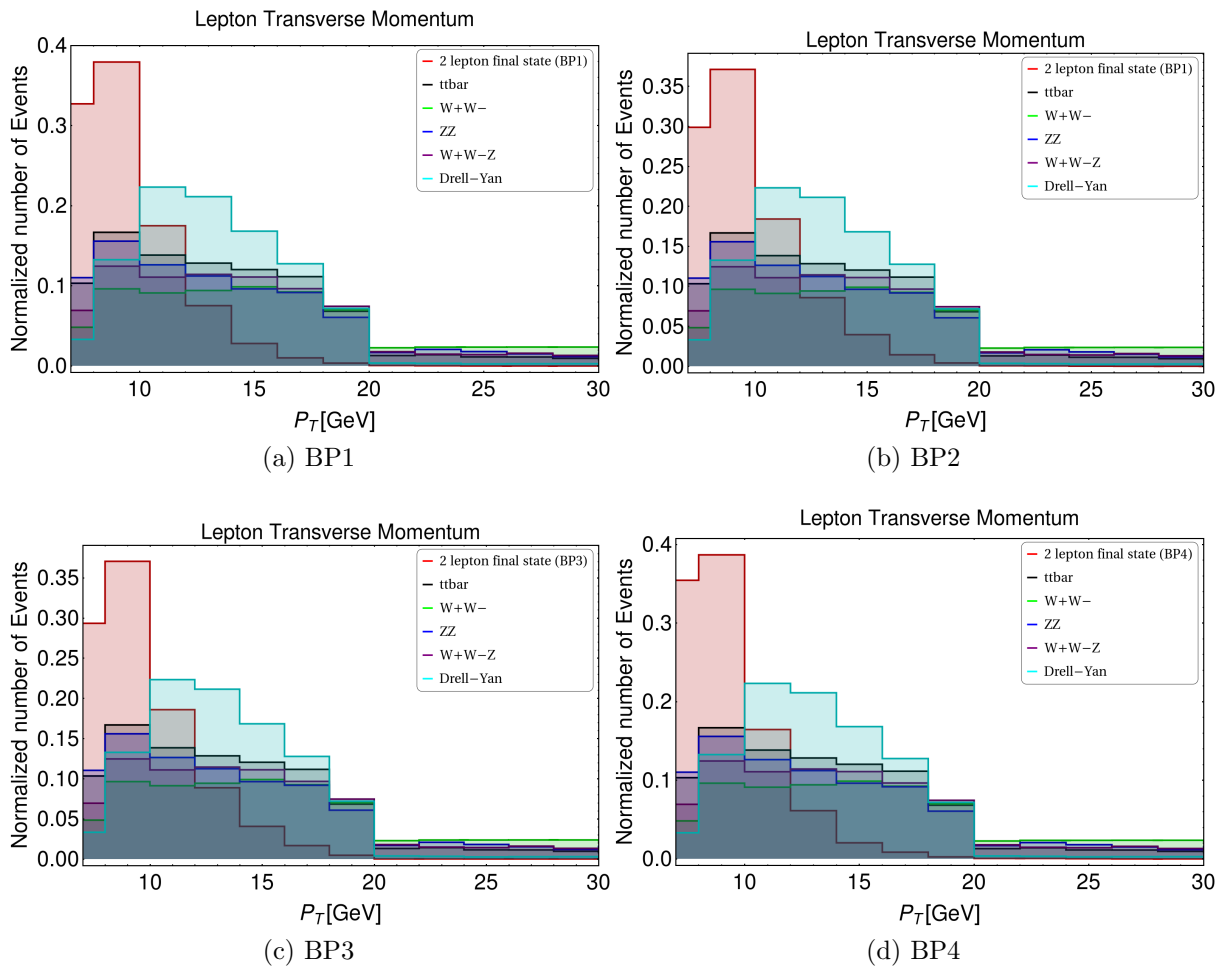


Figure B.2: Lepton transverse momentum (p_T) distributions for all benchmark points

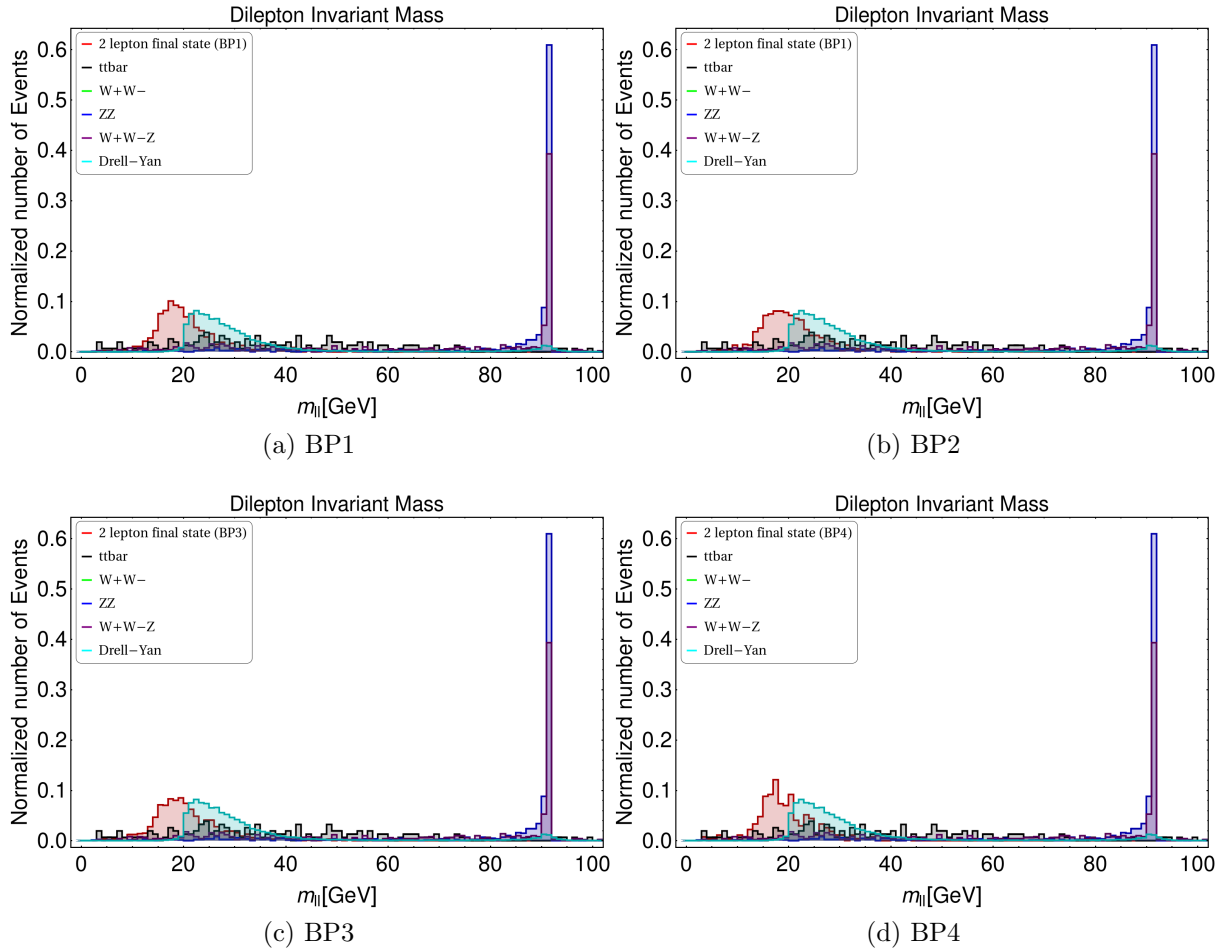


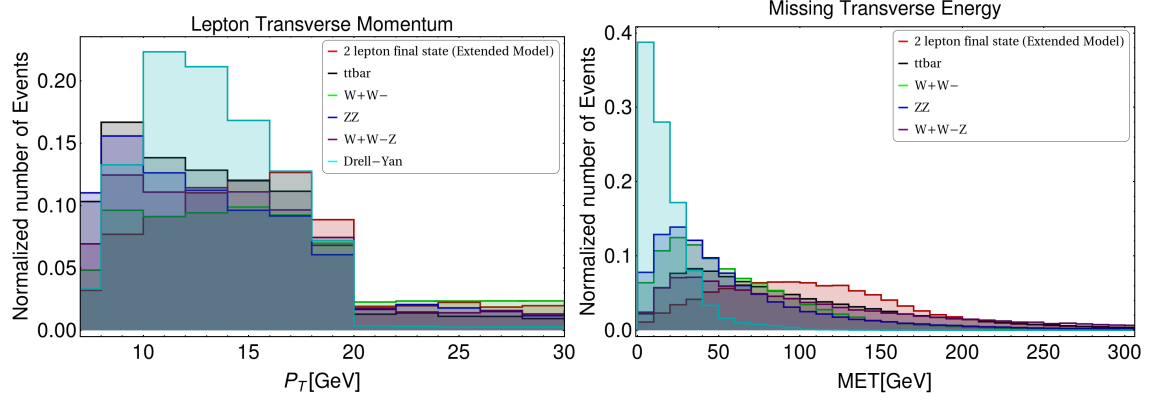
Figure B.3: Dilepton invariant mass (m_{ll}) distributions for all benchmark points

Appendix C

Scalar Triplet Extension to SDFDM model

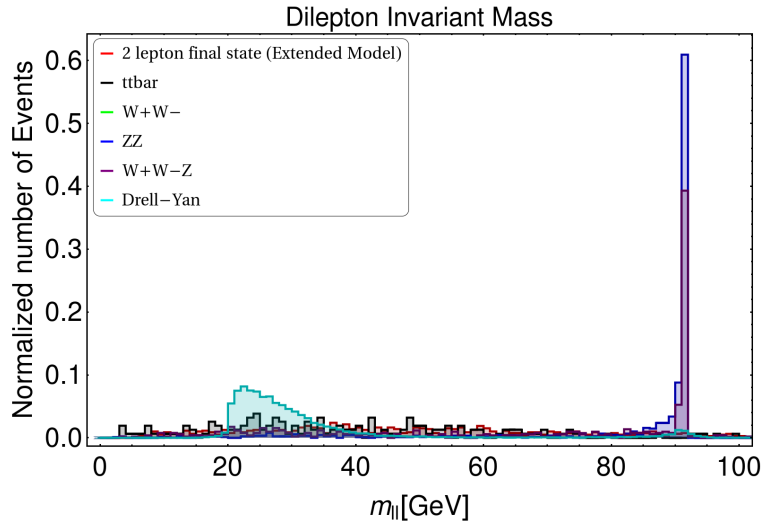
A possible extension to the model can be thought with an additional scalar triplet [62]. This will generate a splitting in the lightest DM fermion states and therefore kinematically forbid the Z mediated interaction. This alternate version will have the freedom of choosing larger mixing angle. Also, in this model the mass difference ΔM can be chosen freely, by adjusting the scalar triplet mass accordingly, such that the chosen benchmark point lies within the resonance region in relic density calculations.

Since the addition of the scalar triplet does not alter the phenomenology largely except for the direct search restrictions, we can proceed to analyze the singlet-doublet fermionic dark matter model without the scalar triplet in the context of collider search signal for the benchmark point from the model extended with the scalar triplet. In Figure C.1, we have shown the distributions for one such benchmark point (along with BP0) with $M_1 = 65$ GeV, $\Delta M = 100$ GeV and $\sin\theta = 0.2$, for opposite sign dilepton final state. Unlike minimal model, the mediating vector bosons in these final states will be on-shell. Figure C.1b, confirms with our argument of missing energy given earlier, as we can see the dominating over SM background at large missing energies.



(a) Lepton transverse momentum (p_T)

(b) Missing transverse energy (MET)



(c) Dilepton invariant mass (m_{ll})

Figure C.1: Distributions for a benchmark point in the extension model allowed by relic density and direct detection constraints given by $M_{\psi_1} = 65$ GeV, $\Delta M = 100$ GeV and $\sin \theta = 0.2$. The beam center of mass energy is 14 TeV and the distributions are for opposite dilepton final state. Final leptons are selected with $p_T > 7$ GeV, $\eta < 2.5$, $R_{ll} > 0.2$, $R_{lj} > 0.4$ and $R_{jj} > 0.4$

Bibliography

- [1] F. Zwicky, “Republication of: The redshift of extragalactic nebulae,” *General Relativity and Gravitation*, vol. 41, pp. 207–224, jan 2009.
- [2] S. van den Bergh, “The Early History of Dark Matter,” *Publications of the Astronomical Society of the Pacific*, vol. 111, pp. 657–660, jun 1999.
- [3] H. W. Babcock, “The rotation of the Andromeda Nebula,” *Lick Observatory Bulletins*, vol. 19, pp. 41–51, 1939.
- [4] V. C. Rubin, “One Hundred Years of Rotating Galaxies¹,” *Publications of the Astronomical Society of the Pacific*, vol. 112, pp. 747–750, jun 2000.
- [5] S. Smith, “The Mass of the Virgo Cluster,” *The Astrophysical Journal*, vol. 83, p. 23, jan 1936.
- [6] J. P. Ostriker and P. J. E. Peebles, “A Numerical Study of the Stability of Flattened Galaxies: or, can Cold Galaxies Survive?,” *Astrophysical Journal*, vol. 186, p. 467, 1973.
- [7] D. Fabricant, M. Lecar, and P. Gorenstein, “X-ray measurements of the mass of M87,” *The Astrophysical Journal*, vol. 241, p. 552, oct 1980.
- [8] R. Massey, T. Kitching, and J. Richard, “The dark matter of gravitational lensing,” *Reports on Progress in Physics*, vol. 73, p. 086901, aug 2010.
- [9] D. Clowe, M. Bradač, A. H. Gonzalez, M. Markevitch, S. W. Randall, C. Jones, and D. Zaritsky, “A Direct Empirical Proof of the Existence of Dark Matter,” *The Astrophysical Journal*, vol. 648, pp. L109–L113, sep 2006.
- [10] G. Arcadi, M. Dutra, P. Ghosh, M. Lindner, Y. Mambrini, *et al.*, “The Waning of the WIMP? A Review of Models, Searches, and Constraints,” *arXiv:1703.07364 [astro-ph, physics:hep-ex, physics:hep-ph, physics:hep-th]*, mar 2017.
- [11] E. L. Wright, J. C. Mather, C. L. Bennett, E. S. Cheng, R. a. Shafer, *et al.*, “Preliminary spectral observations of the Galaxy with a 7 deg beam by the Cosmic Background Explorer (COBE),” *The Astrophysical Journal*, vol. 381, p. 200, nov 1991.

- [12] N. Jarosik, C. L. Bennett, J. Dunkley, B. Gold, M. R. Greason, *et al.*, “7 Year Wilkinson Microwave Anisotropy Probe (WMAP) Observations: Sky Maps, Systematic Errors, and Basic Results,” *The Astrophysical Journal Supplement Series*, vol. 192, p. 14, feb 2011.
- [13] Planck Collaboration, “Planck 2013 results. XVI. Cosmological parameters,” *Astronomy & Astrophysics*, vol. 571, p. A16, mar 2013.
- [14] G. R. Blumenthal, S. M. Faber, J. R. Primack, and M. J. Rees, “Formation of galaxies and large-scale structure with cold dark matter,” *Nature*, vol. 311, pp. 517–525, oct 1984.
- [15] K. Jedamzik and M. Pospelov, “Particle Dark Matter and Big Bang Nucleosynthesis,” in *Particle Dark Matter: Observations, Models and Searches*, pp. 547–564, 2010.
- [16] J. L. Feng, “Dark Matter Candidates from Particle Physics and Methods of Detection,” *Annual Review of Astronomy and Astrophysics*, vol. 48, pp. 495–545, aug 2010.
- [17] F. D. Steffen, “Dark-matter candidates,” *The European Physical Journal C*, vol. 59, pp. 557–588, jan 2009.
- [18] M. Lisanti, “Lectures on Dark Matter Physics,” in *New Frontiers in Fields and Strings*, pp. 399–446, WORLD SCIENTIFIC, jan 2017.
- [19] J. L. Feng, “Dark matter at the Fermi scale,” *Journal of Physics G: Nuclear and Particle Physics*, vol. 32, pp. R1–R24, jan 2006.
- [20] T. M. Undagoitia and L. Rauch, “Dark matter direct-detection experiments,” *Journal of Physics G: Nuclear and Particle Physics*, vol. 43, p. 013001, jan 2016.
- [21] J. Liu, X. Chen, and X. Ji, “Current status of direct dark matter detection experiments,” *Nature Physics*, vol. 13, pp. 212–216, mar 2017.
- [22] LUX Collaboration, “The Large Underground Xenon (LUX) experiment,” *Nuclear Instruments and Methods in Physics Research Section A: Accelerators, Spectrometers, Detectors and Associated Equipment*, vol. 704, pp. 111–126, mar 2013.
- [23] “Dark matter results from 54-ton-day exposure of pandax-ii experiment,” *Phys. Rev. Lett.*, vol. 119, p. 181302, Oct 2017.
- [24] D.-M. Mei and A. Hime, “Muon-induced background study for underground laboratories,” *Physical Review D*, vol. 73, p. 053004, mar 2006.
- [25] A. Minamino, “XMASS experiment, dark matter search with liquid xenon detector,” *Nuclear Instruments and Methods in Physics Research Section A: Accelerators, Spectrometers, Detectors and Associated Equipment*, vol. 623, pp. 448–450, nov 2010.

- [26] M. Kuźniak *et al.*, “DEAP-3600 Dark Matter Search,” *Nuclear and Particle Physics Proceedings*, vol. 273-275, pp. 340–346, apr 2016.
- [27] SuperCDMS Collaboration, “Search for Low-Mass Weakly Interacting Massive Particles with SuperCDMS,” *Physical Review Letters*, vol. 112, p. 241302, jun 2014.
- [28] K.-J. Kang, J.-P. Cheng, J. Li, Y.-J. Li, Q. Yue, *et al.*, “Introduction to the CDEX experiment,” *Frontiers of Physics*, vol. 8, pp. 412–437, aug 2013.
- [29] J. Barreto, H. Cease, H. Diehl, J. Estrada, B. Flaugher, *et al.*, “Direct search for low mass dark matter particles with CCDs,” *Physics Letters B*, vol. 711, pp. 264–269, may 2012.
- [30] CRESST Collaboration, “The CRESST dark matter search,” *Astroparticle Physics*, vol. 12, pp. 107–114, oct 1999.
- [31] PICO Collaboration, “Dark Matter Search Results from the PICO-2L C_3F_8 Bubble Chamber,” *Physical Review Letters*, vol. 114, p. 231302, jun 2015.
- [32] J. Conrad, “Indirect detection of wimp dark matter: a compact review,” *arXiv preprint arXiv:1411.1925*, 2014.
- [33] Fermi-LAT Collaboration, “The Large Area Telescope on the Fermi Gamma-Ray Space Telescope Mission,” *The Astrophysical Journal*, vol. 697, pp. 1071–1102, jun 2009.
- [34] HESS Collaboration, “Observations of the Crab nebula with HESS,” *Astronomy & Astrophysics*, vol. 457, pp. 899–915, oct 2006.
- [35] MAGIC Collaboration, “Performance of the MAGIC stereo system obtained with Crab Nebula data,” *Astroparticle Physics*, vol. 35, pp. 435–448, feb 2012.
- [36] J. Holder, V. A. Acciari, E. Aliu, T. Arlen, M. Beilicke, *et al.*, “Status of the VERITAS Observatory,” in *AIP Conference Proceedings*, pp. 657–660, AIP, oct 2008.
- [37] P. Picozza, A. Galper, G. Castellini, O. Adriani, F. Altamura, *et al.*, “PAMELA A payload for antimatter matter exploration and light-nuclei astrophysics,” *Astroparticle Physics*, vol. 27, pp. 296–315, apr 2007.
- [38] AMS Collaboration, “First Result from the Alpha Magnetic Spectrometer on the International Space Station: Precision Measurement of the Positron Fraction in Primary Cosmic Rays of 0.5350 GeV,” *Physical Review Letters*, vol. 110, p. 141102, apr 2013.
- [39] IceCube Collaboration, “First year performance of the IceCube neutrino telescope,” *Astroparticle Physics*, vol. 26, pp. 155–173, oct 2006.
- [40] ANTARES Collaboration, “ANTARES: The first undersea neutrino telescope,” *Nuclear Instruments and Methods in Physics Research Section A: Accelerators, Spectrometers, Detectors and Associated Equipment*, vol. 656, pp. 11–38, nov 2011.

- [41] G. HERTEN, “THE FIRST YEAR OF THE LARGE HADRON COLLIDER: A BRIEF REVIEW,” *Modern Physics Letters A*, vol. 26, pp. 843–855, apr 2011.
- [42] A. Hoecker, “Physics at the LHC Run-2 and Beyond,” nov 2016.
- [43] F. Halzen and A. D. Martin, *Quark & Leptons: An Introductory Course In Modern Particle Physics*. John Wiley & Sons, 2008.
- [44] M. Cirelli, N. Fornengo, and A. Strumia, “Minimal dark matter,” *Nuclear Physics B*, vol. 753, no. 1, pp. 178 – 194, 2006.
- [45] K. Y. Lee, Y. G. Kim, and S. Shin, “Singlet fermionic dark matter,” *Journal of High Energy Physics*, vol. 2008, no. 05, p. 100, 2008.
- [46] E. W. Kolb and M. S. Turner, *The Early Universe*. Avalon Publishing, 1994.
- [47] K. Griest and D. Seckel, “Three exceptions in the calculation of relic abundances,” *Phys. Rev. D*, vol. 43, pp. 3191–3203, May 1991.
- [48] S. Bhattacharya, B. Karmakar, N. Sahu, and A. Sil, “Flavor origin of dark matter and its relation with leptonic nonzero θ_{13} and dirac cp phase δ ,” *Journal of High Energy Physics*, vol. 2017, p. 68, May 2017.
- [49] G. Blanger, F. Boudjema, A. Pukhov, and A. Semenov, “Dark matter direct detection rate in a generic model with micromegas 2.2,” *Computer Physics Communications*, vol. 180, no. 5, pp. 747 – 767, 2009.
- [50] S. Bhattacharya, N. Sahoo, and N. Sahu, “Minimal vectorlike leptonic dark matter and signatures at the LHC,” *Physical Review D*, vol. 93, p. 115040, jun 2016.
- [51] T. Abe, R. Kitano, and R. Sato, “Discrimination of dark matter models in future experiments,” *Physical Review D*, vol. 91, p. 095004, may 2015.
- [52] B. Schmidt, “The High-Luminosity upgrade of the LHC: Physics and Technology Challenges for the Accelerator and the Experiments The High-Luminosity upgrade of the LHC Physics and Technology Challenges for the Accelerator and the Experiments,” *Hadron Physics IOP Publishing Journal of Physics Conference Series*, vol. 706, 2016.
- [53] T. C. Collaboration, “The CMS experiment at the CERN LHC,” *Journal of Instrumentation*, vol. 3, pp. S08004–S08004, aug 2008.
- [54] J. Adelman-Mccarthy, O. Gutsche, and J. D. Haas, “The CMS Reconstruction Software,” *Journal of Physics Conference Series J. Phys.: Conf. Ser.*, vol. 331.
- [55] A. Alloul, N. D. Christensen, C. Degrande, C. Duhr, and B. Fuks, “FeynRules 2.0 - A complete toolbox for tree-level phenomenology,” *Computer Physics Communications*, vol. 185, pp. 2250–2300, oct 2014.

- [56] J. Alwall, R. Frederix, S. Frixione, V. Hirschi, F. Maltoni, O. Mattelaer, H.-S. Shao, T. Stelzer, P. Torrielli, and M. Zaro, “The automated computation of tree-level and next-to-leading order differential cross sections, and their matching to parton shower simulations,” *Journal of High Energy Physics*, vol. 2014, p. 79, jul 2014.
- [57] J. Alwall, A. Ballestrero, P. Bartalini, S. Belov, E. Boos, and et al., “A standard format for Les Houches Event Files,” *Computer Physics Communications*, vol. 176, pp. 300–304, feb 2007.
- [58] T. Sjöstrand, S. Mrenna, and P. Skands, “A brief introduction to PYTHIA 8.1,” *Computer Physics Communications*, vol. 178, pp. 852–867, oct 2008.
- [59] D. E. Soper, “Parton distribution functions,” *Nuclear Physics B - Proceedings Supplements*, vol. 53, pp. 69–80, feb 1997.
- [60] M. Cacciari, G. P. Salam, and G. Soyez, “The anti-k t jet clustering algorithm,” *Journal of High Energy Physics*, vol. 2008, feb 2008.
- [61] S. Bhattacharya, N. Sahoo, and N. Sahu, “Minimal vectorlike leptonic dark matter and signatures at the LHC,” *Physical Review D*, vol. 93, p. 115040, jun 2016.
- [62] S. Bhattacharya, N. Sahoo, and N. Sahu, “Singlet-doublet fermionic dark matter, neutrino mass, and collider signatures,” *Phys. Rev. D*, vol. 96, p. 035010, Aug 2017.